



Room 14-0551
77 Massachusetts Avenue
Cambridge, MA 02139
Ph: 617.253.5668 Fax: 617.253.1690
Email: docs@mit.edu
<http://libraries.mit.edu/docs>

DISCLAIMER OF QUALITY

Due to the condition of the original material, there are unavoidable flaws in this reproduction. We have made every effort possible to provide you with the best copy available. If you are dissatisfied with this product and find it unusable, please contact Document Services as soon as possible.

Thank you.

Pages are misnumbered

Air-gap sacrificial materials by initiated chemical vapor deposition

by

Long Hua Lee

B. S. Chemical Engineering
National Taiwan University, 1999

M. S. Chemical Engineering
National Taiwan University, 2001

Submitted to the Department of Chemical Engineering
in partial fulfillment of the requirement for the degree of

Master of Science

at the

Massachusetts Institute of Technology

May 2007
[June 2007]

©2007 Massachusetts Institute of Technology

All rights reserved

Signature of Author _____

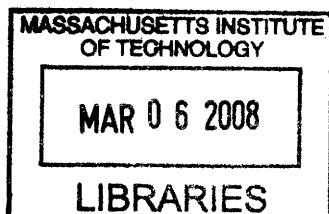
U Department of Chemical Engineering
May 25, 2007

Certified by _____

Karen K. Gleason
Professor of Chemical Engineering
Thesis Advisor

Accepted by _____

Professor William M. Deen
Carbon P. Dubbs Professor
Chairman, Department Committee on Graduate Students



ARCHIVES

Air-gap sacrificial materials by initiated chemical vapor deposition

By

Long Hua Lee

Submitted to the Department of Chemical Engineering
on May 25, 2007 in Partial Fulfillment of the
Requirement of Master of Science

ABSTRACT

P(neopentyl methacrylate-*co*-ethylene glycol dimethacrylate) copolymer, abbreviated as P(npMA-*co*-EGDA), was selected as the potential air-gap sacrificial material among possible combination of twenty monomers and four crosslinkers. P(npMA-*co*-EGDA) was deposited onto substrates using initiated chemical vapor deposition (iCVD) technique. Spectroscopic data showed the effective incorporation of both components in the copolymer and the integrity of repeating units were retained. The onset temperature of decomposition of P(npMA-*co*-EGDA) copolymer could be tuned between 290~350⁰C by varying the composition of the copolymer. The removal rate of polymer was calculated based on interferometry signal-time curve. The activation energy was determined by fitting the rate of decomposition with logistic model and found to be 162.7±8kJ/mole, which was similar to published data. Flash pyrolysis gas chromatography mass spectroscopy analysis showed that the products of thermal decomposition are monomers, rearranged small molecules and low oligomers. The modulus and the hardness were in the range of 3.9 to 5.5 GPa and 0.38 to 0.75 GPa, respectively, and were higher than those of linear poly(methyl methacrylate) (PMMA).

Air-gap structures were constructed in the following scheme: P(npMA-*co*-EGDA) was deposited on the substrate by iCVD, followed by spincoating PMMA electron beam resist and scanning electron beam lithography to implement patterns on the resist. Reactive ion etching (RIE) was then applied to simultaneously etch the PMMA resist and P(npMA-*co*-EGDA) sacrificial material away in a controlled manner, leaving the patterned sacrificial material on the substrate. A layer of porous silica was deposited to cover the substrate and the patterned sacrificial material by plasma-enhanced chemical vapor deposition (PECVD) at 250⁰C and the sample was thermally annealed to allow the decomposed fragments to diffuse through the overlayer of silica. Using the scheme described above, it was possible to construct air-gap structures with feature size of 200nm and feature height of 100nm.

Thesis Supervisor: Karen K. Gleason

Title: Alexander and I. Michael Kasser Professor of Chemical Engineering

Acknowledgement

Looking back at the bumpy path I have tramped through during the three years at MIT, it is extremely difficult for me to say in a decisive manner that the decision of accepting the admission offer I made three years ago was a correct one at this moment. Nevertheless, I would like to offer thankfulness wholeheartedly to those who gave me a boost during the odyssey or on the brink of the abyss of desperation.

I would like to thank my thesis advisor Prof. Karen Gleason, who is never short of good and novel ideas, for her helpful guidance and generous support. It has been a pleasure for me to do research in her group and will always be.

I would also like to thank Dr. Kurt Broderick, who has been such a great help not only in RIE and PECVD but also in useful suggestions on many steps of construction of air-gaps, the long wait for tuning and stabilizing the good old PlasmaTherm was always made pleasant because of his timely appearance in EML; Dr. Mark Mondol, facility manager of scanning electron beam lithography at research laboratory of electronics, for his patience during the training sessions and answering all the naïve questions on fabrication and use of e-beam writer; Dr. Jim Carnaham, for his help on flash pyrolysis-GCMS and response to numerous questions on conducting diffusion experiments in TGA-MS; Dr. Steven Kooi, for his help on BET instrument at ISN. Ms. Libby Shaw for her assistance on XPS experiments and analysis. Special thanks to Dr. Yong Zhang at CMSE for his help on obtaining high quality SEM images of air-gap structures.

Many thanks to the people in Gleason group: W. Shannan O'Shaughnessy, who introduced me to the world of iCVD and showed me how to use FTIR and ellipsometer as well as generously shared his reactor with me; Tyler Martin, for his invaluable help on Charlotte, dry pump and SEM; Wyatt Tenhaeff, for his help on Maximus and the time for designing the filament holder for 8-inch wafer, not to mention the help with my necktie during ACS meeting; Sreeram Vaddiraju, for his creativity and humor that brightens the day and nights in the lab; Kenneth Lau, for his instructions on ITS; Mustafa Karaman for spending lots of time trying to help me with optical microscope and AFM at ISN, Sal Baxamusa for his help on optical microscope in 66-421; Chia-Hua Lee and Núria Marí Buyé for listening to my complains about the workload. Also I would like to thank Sung Gap Im, Malancha Gupta, Kyle Stephen and David Kuster for useful and interesting discussions. It has been such a good time and pleasure to be able to work with these guys that I cannot help smiling and indulging in the great moments in the lab and office though I know I have to finish the part of acknowledgement as fast as I can since I've got experiments to finish.

As an international student who is still pretty bad in English language, makes frequent and abrupt stops when he talks in order to fetch a correct noun or an appropriate adjective after staying in the US for almost three years, one of my best achievements in MIT, as far as I am concerned, is make friends outside the office and lab. Over the three year, I had three best friends on MIT campus: Alfonso Villanueva, Yuki Hori and Ryan Odegard; their presence led me to believe that the god, if ever in existence, might be cruel to one in a certain aspect but will be kind in others. Gracias mi amigo Alfonso, por ayudarme en aspectos varios, no sé que cuando y donde vamos a vernos otra vez pero estoy cierto que si; arigatou Yuki, itsumo sewa ni natte kudaisaru koto, soshite boku o hakemasu koto, Yuki no koto o wasurenai yo; and Ryan, thanks for expanding my horizon on American culture, sports, jazz music and embarrassing me a great deal by laughing aloud when I said some like "horse hockey" for "polo" and "transfer the ball" instead of "pass the ball". Again guys, it's you who made the good

days more enjoyable and the frustrating ones less painful. Three best friends in three years, that's priceless already. Ikuo and Mami Taniguchi for their patience of my lousy Japanese, Sezen Curgul for her encouragement during our struggles to make it to the second oral qual, Ayse Asatekin for her help in the previous research group, Leonardo Shieh and Rohit Narula for their humor which made life smoother...there are so many people that I should offer my thankfulness and I believed I was really blessed to get to know them.

And finally, I would like to thank and say sorry to my parents who have been supporting me incessantly over these years, regardless of the undeniable fact that their son let them down. Whenever I talked to them over the phone, I could feel that their care and love for me are drifting toward me through the phone line although at times I am not resonating with those and I feel bad about myself, for they took great pain to send me to MIT.

.....

I love and detest writing acknowledgements because it tends to get me into these old memories, wonderful or terrible. Although the second law of thermodynamics cannot be violated and people have to part eventually, great memories are not governed by entropy and always linger. And yes, during these three years, I did it my way, with the help of lots of people, and I wish you all the best.

Table of Contents

Abstract.....	3
Acknowledgement.....	4
Table of Content.....	6
List of Figure.....	8
List of Table.....	10
List of Scheme.....	11
Background and Introduction	
Challenge imposed by International Technology Roadmap for Semiconductors (ITRS).....	12
Air-gap construction.....	13
Thermal degradation behavior of polymers.....	14
Criteria for selection of air-gap sacrificial polymeric materials.....	15
Polymerization using iCVD.....	16
Experimental	
Strategies.....	18
Potential candidates of monomers.....	19
Potential candidates of crosslinking monomers.....	22
Materials.....	23
Instrumentation.....	23
Results and Discussions	
Thermal properties of homopolymer of selected monofunctional monomer.....	34
Thermal properties of homopolymer of selected bifunctional monomer.....	36
Copolymerization of selected monomers and crosslinkers.....	38
Characterization of P(npMA-co-EGDA)	
IR spectra of P(npMA-co-EGDA) and curve fitting of characteristic peaks.....	41
Nuclear Magnetic Resonance spectra of P(npMA).....	44
XPS of deposited thin film: P(npMA), P(EGDA) and P(npMA-co-EGDA).....	46
ITS characterization of polymer thin films on substrates.....	49
Onset temperature on decomposition and calculation of removal percentage.....	51
Kinetic data of thermal decomposition: removal rate and activation energy.....	53
Flash pyrolysis gas chromatography mass spectroscopy.....	61
Residue on substrate after thermal degradation: FTIR and XPS analysis.....	72

Nanoindentation: Young's modulus and hardness.....	75
Construction of air-gap structure using e-beam lithography.....	78
Conclusion.....	80
Reference.....	81

List of Figures

Figure 1.	Temperature programming in ITS experiments.....	27
Figure 2.	Typical loading and unloading curves in nanoindentation test; fused silica used as standard	31
Figure 3.	Nanoindentation loading-unloading curves of P(npMA-co-EGDA).....	31
Figure 4.	Optimized structure of (A) npMA and (B) CPMA monomer.....	40
Figure 5.	FTIR spectra of monomer and homopolymer of npMA and EGDA and copolymer thereof	41
Figure 6.	Comparison of iCVD and commercial P(npMA) polymerized via free radical pathway...	43
Figure 7.	FTIR spectra of P(npMA-co-EGDA) copolymer.....	43
Figure 8.	¹ H NMR of npMA and Poly(npMA); CDCl ₃ used as deuterated solvent.....	44
Figure 9.	XPS diagram and curve fitting result on P(npMA).....	46
Figure 10.	XPS diagram and curve fitting result on P(EGDA).....	47
Figure 11.	XPS survey and high resolution scan on carbon and oxygen of P(npMA-co-EGDA), F _{npMA} = 1.0 sccm.....	47
Figure 12.	Typical ITS diagram and the determination of onset temperature of degradation.....	50
Figure 13.	Variation of interferometry signal (and thus thickness) with time.....	50
Figure 14.	Photograph of polymer samples deposited on silicon wafer after ITS test: (1) Bare silicon wafer, (2) P(npMA), (3) P(npMA-co-EGDA), F _{npMA} =1.75sccm, (4) P(npMA-co-EGDA), F _{npMA} =1.5sccm, (5) P(npMA-co-EGDA), F _{npMA} =1.25sccm, (6) P(npMA-co-EGDA), F _{npMA} =1.0sccm, (7) P(npMA-co-EGDA), F _{npMA} =0.75sccm, (8) P(EGDA).....	51
Figure 15.	Effect of flowrate of npMA on the onset temperature of thermal degradation and removal percentage.....	53
Figure 16.	Variation of thickness versus time of thermal decomposition of P(npMA-co-EGDA), F _{npMA} = 1.0sccm.....	56
Figure 17.	Plot of normalized thickness versus time in ITS experiments for P(npMA-co-EGDA) copolymers.....	56
Figure 18.	Arrhenius plot of removal rate versus temperature.....	59
Figure 19.	Activation energy of removal of P(npMA-co-EGDA) versus flowrate of npMA.....	60
Figure 20.	GC chromatogram of npMA and EGDA monomers.....	62
Figure 21.	MS spectra of npMA (m.w.: 156 Da).....	62
Figure 22.	MS spectra of npMA (m.w.: 170 Da).....	62

Figure 23. GC chromatogram of decomposition product of P(npMA).....	63
Figure 24. MS spectra of the peak at 10.617min.....	63
Figure 25. MS spectra of the peak at 17.438min.....	63
Figure 26. GC chromatogram of decomposition product of P(EGDA).....	65
Figure 27. Percentage of peak area of P(EGDA) decomposition products in GCMS analysis.....	65
Figure 28. GC chromatogram of decomposition product of P(npMA-co-EGDA).....	67
Figure 29. Percentage of peak area of P(npMA-co-EGDA) decomposition products in GCMS analysis	67
Figure 30. TGA thermogram of P(EGDA).....	68
Figure 31. TGA thermogram of P(npMA-co-EGDA).....	69
Figure 32. TGA thermogram of P(npMA).....	69
Figure 33. FTIR and XPS results of residue on silicon wafer after thermally-treated at 400C for 1hr under N ₂	72, 73
Figure 34. (A) Fitting of P(npMA-co-EGDA) before ITS, (B) Fitting of the same sample after ITS...	74
Figure 35. Effect of flowrate of npMA on the Young's modulus and hardness of copolymers.....	76
Figure 36. SEM image of air gap with feature size of 200nm and feature height of 100nm.....	79

List of Tables

Table 1. Potential candidates of monomer.....	20, 21
Table 2-1. Conditions of deposition of various monomers.....	28
Table 2-2. Onset temperatures of degradation of thin films deposited on silicon wafer (T_d) and removal percentages of homopolymers consisting of selected monomer.....	35
Table 3. Potential candidates of crosslinkers.....	37
Table 4. Onset temperatures of degradation of thin films deposited on silicon wafer (T_d) and removal percentages of homopolymers consisting of selected crosslinkers.....	38
Table 5. Onset temperature of thermal degradation, removal percentage and deposition rate of selected copolymers.....	39
Table 7. Ratio of total peak area of carbon (C1s) and oxygen (O1s) in high resolution scan in XPS	49
Table 8. Onset temperature of decomposition and removal percentage after heating at 400C for 1 hr	52
Table 9. Fitting parameters of removal rate time (<u>without</u> thickness normalization).....	57
Table 10. Fitting parameters of removal rate time (<u>with</u> thickness normalization).....	57
Table 11. Removal rate (um/min), pre-exponential factor and activation energy at selected temperatures.....	58
Table 12. Removal rate (um/min), pre-exponential factor and activation energy at selected Temperatures.....	58
Table 13. Results of flash pyrolysis of homo- and copolymers of P(npMA-co-EGDA).....	71
Table 14. Young's moduli and hardnesses of P(npMA-co-EGDA).....	76

List of Schemes

Scheme 1.	Flowchart of fitting of “residual thickness versus time” curve.....	55
Scheme 2.	Flowchart of construction of air-gap structure using e-beam lithography.....	78

Challenge imposed by International Technology Roadmap for Semiconductors (ITRS)

According to International Technology Roadmap for Semiconductors, also known as Moore's Law, the number of transistors on a wafer has increased by more than six orders of magnitude in the past 35 year and is still increasing. However as the density of transistors increases, the problem of downsizing are encountered as the feature size proceeds to deep submicron regime, such as RC (resistance-capacitance) delay, an increase in RC constant and results in deterioration of the performance, most notably in the forms of insufficient heat dissipation, electromigration, crosstalk, etc. Therefore new materials and/or fabrication processes are in dire need. Aluminum, the conventional conducting material in integrated circuit, has been replaced by copper, which has a lower resistivity (60% of that of aluminum), higher heat conductivity and lower tendency of undergoing electromigration, a phenomenon that atoms tend to drift parallel to the direction of electric field and can eventually cause voids in the circuit and failure of the device.

The conventional dielectric material silica dioxide, has a dielectric constant of 4.0~4.2 and suffices the device with feature size of 0.25 to 2 micron⁴⁹. However, as the feature size reduces in dimension, materials with lower dielectric constants are required in order not to cause crosstalk or loss of fidelity of the signals. Over the past two decades, materials with lower dielectric constants (low k) have been developed and some of them have been commercialized, such as fluorinated silicate glass (FSG), organic silicate glass (OSG), fluorinated organic materials (FOM) and porous materials. Depending on the amount of porogens incorporated, the dielectric porous materials can be as low as 1.1 to 1.5 after thermal degradation of these porogens, usually consisting of polymers. However, porous materials have serious integration problems such as poor thermal and mechanical performance, migration of copper into the pores, etc. Techniques such as pore sealing by treating the surface of porous materials with plasma to prevent infiltration of copper atoms have been developed; however, more problems

such as carbon depletion at the surface that leads to the undesired increase of dielectric constant have been observed and limit their the practical use. Nevertheless, the concept of effective reduction in dielectric constants by incorporating voids in dense materials implies the possibility of using of air as the ultimate dielectric material, if other properties are not compromised appreciably.

Air-gap construction

Two primary techniques of formation of air-gap structure have been under extensive investigation: non-conformal chemical vapor deposition and incorporation of sacrificial materials^{47, 48}. The former requires the formation of intermetal trenches on the same layer, followed by non-conformal deposition so that isolation of air is eventually achieved due to the closure of the deposited species and acts as dielectric materials. Non-conformal chemical vapor deposition was first discovered between two aluminum lines and deemed detrimental to integrated circuit reliability but was later found out to be an affective approach to reduce the dielectric constant. Because of the non-conformal nature, the shape of the air-gap structure looks like a key-hole; the widest part is at the bottom and the distance between the sidewall gradually reduces to close the gap. Silicon nitrides or silicon oxides are two of the choices for the deposition.

On the other hand, sacrificial materials are deposited and patterned in the early stage of the fabrication flowchart, followed by passivation of the periphery of sacrificial materials, electroplating of copper, chemical mechanical polishing (CMP), and thermally degrade the sacrificial material as the last step. Thus sacrificial materials play the role of template or “void precursor” and the decomposition products during thermal treatment have to diffuse out of the multilayer assembly. Thermal degradable polymers have been the major option for sacrificial material in this application since the thermal properties are tunable based on the choice of the structure of the main chain or side groups, etc.

Thermal degradation behavior of polymers

The thermal stability and mechanism of thermal degradation of a specific polymer depends on many factors including the chemical composition, the repeating unit(s), the type of endgroups, the molecular weight and the presence of impurities. For example, poly(methyl methacrylate) (PMMA) starts to decompose via a monomer-unzipping mechanism at the temperature of 250 °C and the only product of thermal degradation is the methyl methacrylate monomer unit¹⁻³. In contrast, upon heating, poly(methacrylic acid) (PAA) forms highly thermally stable poly(methacrylic acid anhydride)^{1,3} by dehydration and cyclization and does not decompose until 500 °C. Furthermore, methyl alcohol, a species that does not appear during thermal degradation of PMMA or PAA, is found among the thermal degradation products of poly(methyl methacrylate-*co*-methacrylic acid)³, indicating a different mechanism taking place in the simultaneous presence of both polymers. Other examples include the catalytic effects of metal ions, the subtle difference in the length or structure of side groups of polymer backbones³.

Degradation of polymer chains takes place at the most thermally vulnerable chemical bonds. Polymers containing weak bonds between carbon and either halogen atoms (except fluorine)^{1-2,4}, thiol or disulphide groups almost always degrade at these sites to form radicals⁵. Examples include poly(vinyl chloride) and poly(vinyl bromide). Fragmentation denotes the cleavage of certain groups from the main polymer backbone and results in a complicated spectrum of degraded products containing the mixture of fragments, monomers and oligomers. If the strengths of the chemical bonds in polymer are approximately the same and formation of a relatively stable macroradical is possible, monomer unzipping is typically the dominant mechanism and the thermally degraded products will be primarily the monomer units². Poly(methyl methacrylate) and poly(alpha-methyl styrene)⁵ are two typical examples in which stable tertiary radicals form via thermal degradation. Poly(methyl acrylate)¹, on the

other hand, does not degrade solely by monomer unzipping since the intermediate is the less stable secondary radicals.

As already discussed for PAA, reactions between side groups can occur during heat treatment. Examples include formation of primary amine of poly(n-alkyl methacrylamide)³, cyclization of cyano groups in polyacrylonitrile³, or beta-hydrogen abstraction by ester oxygen to form carboxylic acids¹⁻³. Most of these reactions lead to higher thermal stability and can be either advantageous or detrimental depending on applications.

Criteria for selection of air-gap sacrificial polymeric materials

Thermally degradable polymeric materials have been suggested⁶⁻⁷ as one of the potential candidates to replace the low dielectric constant materials (low-k materials). The role of the polymeric materials is to serve as a template or the so-called sacrificial materials. When subjected to sufficient thermal energy, the thermally labile polymers degrade to small molecules products which diffuse away, creating a void of the same shape in its place. Currently the low-k materials used extensively in the electronic and semiconductor industries have dielectric constants ranging from 2.0 to 4.0. Specific examples include silica (k = 4.0), fluoro-silicon glass (k = 3.2~3.7), organo-silicon glass (k = 2.7~3.0) and fluorocarbon materials (k = 2.0~2.7). However, if the line density and number of transistors per unit area in integrated circuits (IC) are to increase as predicted by Moore's Law⁸, new dielectric materials are demanded in order to reduce the delay in transmitting signals from one transistor to another, suppress the extensive crosstalk between neighboring circuits and to reduce overall power consumption.

Air/vacuum has the lowest possible dielectric constant of 1.0, and low-k materials having porous structure have been proposed to decrease the k beyond 2.0⁹⁻¹¹. However, porous low-k materials suffer

serious integration problems resulting from reduced mechanical and thermal properties as well as contamination of the porous structure during subsequent process steps¹². Therefore attention has been gradually shifting to the formation of air-gap structures. The benefit of using air-gaps would be most pronounced when applied to most critical parts where the line width and the distance between neighboring lines are lower than 50 nm, and they are essentially free of the problems of pore-sealing, copper contamination, heat accumulation, and the mechanical properties of largely retained.

Since the sacrificial materials for air-gap will be decomposed to form air-gaps as one of the later steps in fabrication in the IC, the sacrificial material must display solvent resistance, thermal stability and mechanical strength in order to withstand subsequent processing steps. Numerous acids, bases and organic solvents are used in IC process, and the sacrificial materials must retain their original dimensions regardless of the presence of these chemicals. Dissolution of sacrificial materials or swelling should be rigorously controlled or excluded. Chemical vapor deposition of barrier layers on top of the sacrificial materials is anticipated to take place at substrate temperature between 250~320 °C. Hence, the sacrificial materials must be thermally stable in this range. Furthermore, the percentage of residue left on the substrate should be minimized to guarantee proper electrical performance. The species of thermally-degraded products and the residues are also to be taken into consideration when choosing the sacrificial material since the size of the volatile products will determine the rate and the percentage of diffusion. High value of hardness and moderate Young's modulus are required to allow steps such as chemical mechanical polishing and flip chip bonding.

Polymerization using iCVD

Most polymerization processes, including synthesis and purification (precipitation and dissolution of polymers in non-solvent and good solvent, respectively), are generally conducted in common organic

solvents to achieve uniform distribution of monomers and prevent too high a reaction rate as is the usual case for bulk polymerization and to enhance the purity of desired product by utilizing the solubility difference. However, common organic solvents are moderately or highly volatile and harmful for organism; acute exposure to large amount of solvent can cause irreversible damage to body tissues or even death. The amount of solvent is usually much larger than the reactive monomers thus careful processing and proper disposal of these solvents are required. Use of solvent in some processes such as spin casting of polymers onto substrates with high aspect ratios or small feature size can result in non-uniform coating as a result of surface tension problems³⁵. Additionally, in spin casting only a few percent of dispersed materials remains on the wafer. The majority of the material of which is cast off from the edge³⁶ of the substrate must be disposed of as hazard waste.

Initiated chemical vapor deposition (iCVD)³⁴ is a polymerization process without any use of solvents. The initiator and monomer(s) are heated in a vacuum system at moderate temperatures and the vapors of initiator and monomer(s) are mixed well in the channel before they enter the reaction chamber. Upon contact to a set of resistively-heated filament in the chamber, the initiators dissociate into two free radicals. The free radicals along with the monomer molecules are adsorbed onto the substrate where surface polymerization takes place. With iCVD process, no solvent is required and deposition of various polymers onto any surface, including those with small size feature and high aspect ratios, is made straightforward. Deposition of highly crosslinked polymer onto substrate is also possible using iCVD whereas it is extremely difficult for solution process. Deposition processes of fluoropolymers³¹, antimicrobial surface coating³², hydrogels, insulation materials³³, random and block copolymers onto flat or patterned surface have been reported or are under investigation. In this thesis, copolymers are deposited onto silicon wafer substrate using iCVD technique.

Strategies

Crosslinked polymers generally have higher chemical resistance as well as thermal stability and mechanical property compared to their linear counterparts due to their rigid structure and the much lower mobility of polymer backbones. Thus, crosslinked polymer will be explored in this thesis as one of the potential candidates for air-gap sacrificial materials.

There are two strategies for synthesis of crosslinked polymers. One involves introduction of two monomers at a time where at least one is multifunctional, followed by the copolymerization of the two species. Poly(styrene-co-divinylbenzene) is an example. The other is polymerization of a single monomer with functional side groups, followed by reaction with externally supplied chemical species or energy so that crosslinks form. Free radical polymerization of poly(4-dimethylmethoxysilylstyrene) followed by sol-gel reaction falls into this category.

The single-monomer strategy is advantageous in that there are no differences in reactivity during polymerization. However, it is often the second step of formation of crosslinks that disfavors the single-monomer strategy. The functional side groups are often different in chemical nature from the polymer backbone and thus the properties of final crosslinked products can be unpredictable. For example, the aliphatic backbone of crosslinked poly(4-dimethylmethoxysilylstyrene) is stable in basic aqueous solution but the siloxane parts are cleaved¹³ in the same solution and the polymer becomes soluble. Another concern with single-monomer strategy is that it required two sequential chemical reactions, the thermodynamic and the kinetic issues of the second crosslinking forming step must not interfere with the first polymerization reaction.

On the other hand, careful selection of reactants for the dual monomer strategy is pivotal to successful

incorporation of both monomers in the final polymers⁶. Monomers with similar reactivity often result in a copolymer containing both species in a proportion that can be directly related to the ratio of monomer feeds. Without proper selection, polymerization using monomers with significantly different reactivities may result in two homopolymers.

In this thesis, both the single and dual monomer strategies will be explored for the synthesis of crosslinked polymeric films for air-gap sacrificial materials.

Potential candidates of monomers

One of the requirements of an ideal sacrificial material for air-gap fabrication is clean decomposition which leaves only a minimal amount of residue behind on the substrate. For this purpose, polymethacrylates are chosen since they are known to decompose cleanly (>99.5%) by monomer-unzipping¹⁻³. Table 1 illustrates the candidates of methacrylate monomers screened which bear various side groups such as phenyls, ethers, silyl/siloxyl groups, amides, unsaturated and saturated hydrocarbon groups. Those depicted by a solid frame are the ones tested using iCVD methodology after careful assessment. Propenyl acetate (IpAc), a homolog of vinyl acetate, was added into iCVD test group. Although P(IpAc) was shown to decompose as cleanly as polymethacrylates in initial thermal degradation tests, the deposition rate was extremely slow (0.2 nm/min) to be of any practical use for polymer thin film formation. The exceptionally high vapor pressure of IpAc (42.5 torr at 25 °C) among the pool of potential monomer candidates is believed to result in intolerably slow deposition rates, because of the low surface concentration of adsorbed IpAc at the tested partial pressure.

The first additional criterion for refining the selection of the monomer to be tested was the absence of beta-hydrogen in the side group. This criterion takes heed of possible beta-hydrogen abstraction in

which the carboxylic acid groups form and the corresponding olefin molecules are released, followed by formation of acid anhydrides which are quite thermally stable. Therefore monomers such as n-butyl methacrylate and tert-butyl methacrylate were not considered¹⁻³.

The next screening consideration was published onset temperatures for polymer decomposition, monomer reactivity and monomer volatility. Among those monomers lacking beta-hydrogens, phenyl and benzyl methacrylate were reported to decompose at undesirably low temperatures of 200 °C¹⁴ and 150 °C¹⁵, respectively. N-alkyl methacrylamides form cyclic structures which are too thermally stable to decompose cleanly during heat treatment^{1,3}, while N,N-dialkyl methacrylamides do not polymerize

Table 1: Potential candidates of monomer

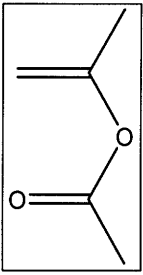
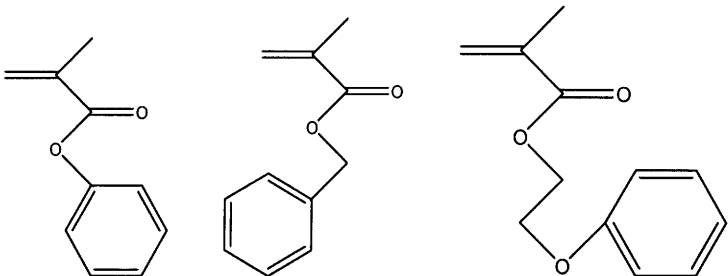
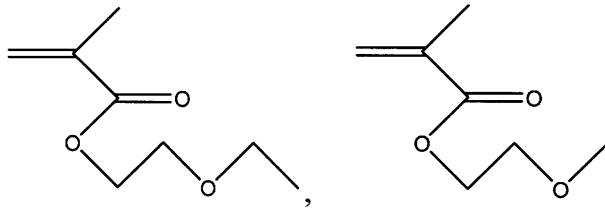
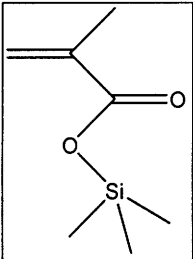
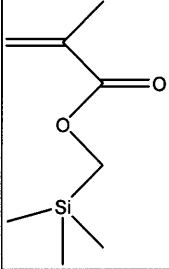
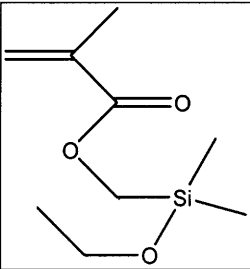
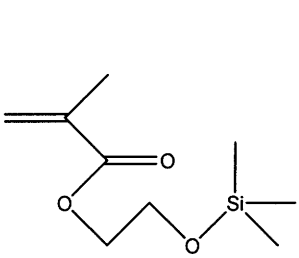
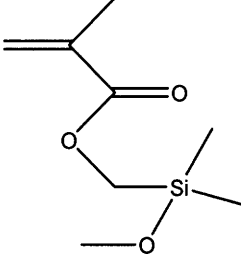
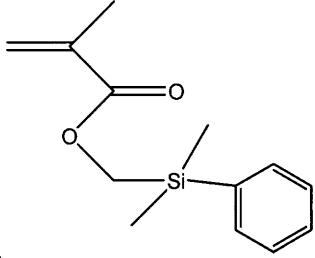
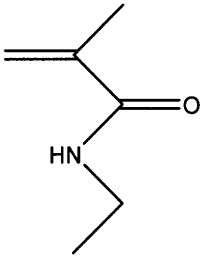
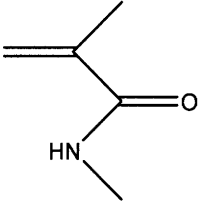
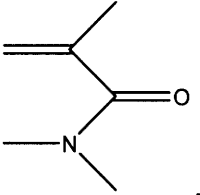
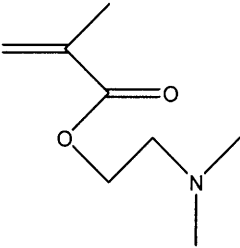
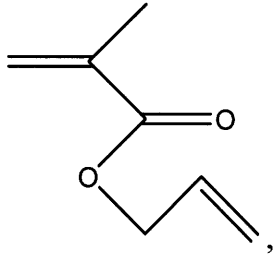
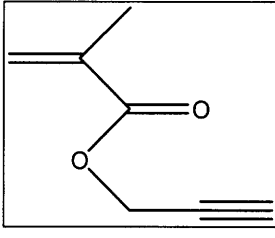
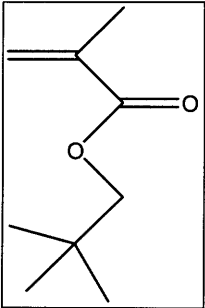
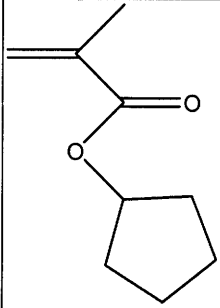
Vinyl ester	
 (IpAc)	
Phenyl group-containing methacrylates	
	
Ether group-containing methacrylates	
	

Table 1 (Cont.): Potential candidates of monomer

Silicon-containing methacrylates	
	(TMA),
	(TMMA),
	(EMSMA)
	,
	,
	
Amine group-containing methacrylates	
	,
	,
	,
	
Methacrylates with unsaturated hydrocarbon side groups	
	,
	(PMA)
Methacrylates with saturated hydrocarbon side groups	
	(npMA),
	(CPMA)

due to steric hindrance in the proximity of radical center¹⁶⁻²¹. Monomers such as

dimethylphenylsilylmethyl methacrylate and adamantyl methacrylate²² (not shown) are not considered for iCVD process because of their extremely low vapor pressures even at elevated temperatures, even though they lack of beta-hydrogens and the poly(adamantyl methacrylate) has been reported to be highly thermally stable with onset temperature of 300~320 °C²².

Potential candidates of crosslinking monomers

For the purpose of efficient incorporation of both monomers and crosslinkers, only difunctional acrylate and methacrylate crosslinker are considered due to their similarity in reactivity. The thermal stabilities of polymer containing crosslinkers with three or more functional groups are expected to be higher than those containing two. However, monomers with more than two vinyl groups generally have insufficient volatility for introduction into the reactor. While heating increases the vapor pressure, this temperature must remain below the self-polymerization or decomposition point of the monomer.

Polyacrylates do not decompose as cleanly as polymethacrylates. Take poly(methyl acrylate) and poly(methyl methacrylate) for example: depending on the final heating temperature, the volatilization percentage of the former ranges from 9.8% at 292 °C to 96.8% at 399 °C after heating for 30 minutes in vacuum², while the volatilization percentage of the latter ranges from 9.9% at 281 °C to 97.2% at 354 °C under the identical conditions². These data show that polymethacrylates decomposed more cleanly than polyacrylates with the same side group. Furthermore, because the formation of secondary free radicals required for polyacrylates decomposition is relatively difficult due to lower degree of hyperconjugation to delocalize the radical center, the polyacrylates are superior in thermal stability to the polymethacrylates³. To determine the most suitable copolymer, the effect of the crosslinker must also be considered. Thus, the next screening step involves both an assessment of the properties of homopolymerized crosslinkers, and then by evaluation of suitable combination of single vinyl

containing monomers and crosslinkers.

Materials

Trimethylsilyl methacrylate (TMA, 98%), ethylene glycol dimethacrylate (EGDMA, 98%), tert-butyl peroxide (TBPO, 98%), methyl isobutyl ketone (MIBK, >99.5%) and isopropanol (IPA, 99.9%) were obtained from Sigma Aldrich. Trimethylsilylmethyl methacrylate (TMMA, >95%) and ethoxydimethylsilylmethyl methacrylate (EMSMA, >95%) were purchased from Gelest Inc. Neopentyl methacrylate (npMA, >98%) and poly (neopentyl methacrylate) (P(npMA)) reference were obtained from Scientific Polymer Products, Inc. Cyclopentyl methacrylate (CPMA, >98%), 1,3-propanediol dimethacrylate (PDDMA, 98%) and 1,3-propanediol diacrylate (PDDA, 98%) were supplied by Monomer-Polymer & Dajac Laboratory Inc.; propargyl methacrylate (PMA, 98%) was provided by Alfa Aesar, deuterated chloroform (CDCl_3 , 99.8% D) was purchased from Cambridge Isotope Laboratory and ethylene glycol diacrylate (EGDA, 98%) was obtained from PolySciences, Inc. PMMA e-beam resist (950PMMA A4, solid content 4% in anisole, molecular weight of PMMA: 950kDa) was purchased from MicroChem. All monomers were checked by proton NMR before subject to reaction and used without further purification.

Instrumentation

1. Initiated Chemical Vapor Deposition (iCVD)

The 200 mm diameter iCVD chamber and accessories has been described elsewhere^{25, 33-35}.

During the screening stage, various deposition conditions were tested, and the following criteria were taken into consideration:

- (1) Heating liquid monomer or crosslinker at elevated temperatures in order to produce very high flowrate of vaporized monomer or crosslinker was undesired due to the possibility of thermally-induced bulk polymerization. The heating temperatures were typically kept lower than 100 °C for all monomers and crosslinkers.
- (2) Condensation of vaporized monomer or crosslinker in the chamber was avoided.

The physical properties of monomers and crosslinkers, such as saturated pressure at a fixed temperature, vary substantially depending on the sizes of molecules and thus the intermolecular interaction. Therefore different deposition conditions were required for different monomers and crosslinkers. The range of deposition conditions are listed below:

- A. Filament temperature: 245~355 °C.
- B. Substrate temperature: 25~45 °C.
- C. Pressure in the reaction chamber: 100~3000 mtorr.
- D. Flowrate(s):
 - (A) Initiator (TBPO): 0.45~1.3 sccm.
 - (B) Monomer (including TMMA, PMA, CPMA, npMA): 1.35~5.2 sccm.
 - (C) Crosslinker (including EGDA, EGDMA, PDDA, PDDMA): 0.4~0.6 sccm.
- E. Filament material: 0.5mm diameter annealed Constanten[®] resistant alloy (Cu 55%, Ni 45%, Goodfellow Cambridge Limited).

Table 2-1 shows the optimal deposition conditions for IpAc, TMMA, npMA, EMSMA, CPMA and PMA. Due to the wide range of physical properties of these monomers, the deposition conditions vary appreciably.

Two monomers (npMA and CPMA) and two crosslinkers (EGDA and EGDMA) were chosen after screening; details are described in the section of “Interferometry for Thermal Stability (ITS) testing on homopolymers”. At this stage, the flowrates of monomers, crosslinkers and TBPO initiators were maintained at 1.125 ± 0.125 sccm, 0.45 ± 0.1 sccm and 0.75 ± 0.25 sccm, respectively. The filament and stage temperature were kept at 280 and 30 °C, respectively. The pressure in chamber was held at 760 mtorr. The flowrate of species X will be abbreviated as F_X hereafter; for example, the flowrate of npMA will be written as F_{npMA} . Poly(neopentyl methacrylate-*co*-ethylene glycol diacrylate), abbreviated P(npMA-*co*-EGDA) hereafter, was determined as the best candidate for air-gap sacrificial material after assessment in thermal properties. At this stage, F_{EGDA} was kept at 0.45 ± 0.1 sccm and F_{TBPO} at 0.7 ± 0.1 sccm while F_{npMA} was steadily increased from 0.75 to 1.75 sccm by 0.25 sccm step to synthesize P(npMA-*co*-EGDA) of five different components. Other deposition conditions, including filament and stage temperatures as well as chamber pressure, remained the same as those in screening process.

Hereafter P(npMA-*co*-EGDA) with the flowrate of npMA equal to 1.0 sccm will be used as the representative copolymer undergoing various types of characterization unless specified.

2. Fourier Transform Infrared Spectroscopy (FTIR)

FTIR spectra were taken using Nexus 870 FTIR. The chamber was flushed with 50 SCFH of nitrogen for at least two minutes before taking spectra on backgrounds and samples. The number of scan was kept at 64 with resolution of 4 cm^{-1} . Silicon wafer or KBr pellet were used as backgrounds for polymer thin films and monomers in liquid state, respectively. The range of measurement was between 4000 and 400 cm^{-1} and base line correction was performed on the spectra of polymer thin films. For reference, 0.5 g of commercial P(npMA) was dissolved in

9.5 g of 4-methyl-2-pentanone (methyl isobutyl ketone, MIBK) and the solution was spun-cast at 1500rpm on silicon wafer, dried at 110 °C for an hour on a hot plate in ambient. The FTIR spectrum of commercial P(npMA) was taken under the same condition as described earlier.

3. Nuclear Magnetic Resonance Spectroscopy (NMR)

Polymer and monomer proton ^1H NMR spectra were taken using Bruker Avance-400. 6 to 8 milligrams of polymer or monomer were added in 0.6 to 0.7 milliliters of deuterated chloroform; the solutions were shaken well before adding into clean NMR tubes. The characteristic peaks of CDCl_3 were at 7.24 and 1.50 ppm and did not interfere with the peaks for the monomer or polymers. The experiments were conducted at 400 MHz and room temperature. Number of scans and acquisition time for npMA are 16 and 4 seconds, and 256 and 5 seconds for iCVD-synthesized P(npMA), respectively. Proton NMR of commercial P(npMA) was taken at the Varian Mercury 300 and room temperature; number of scans and acquisition time were 16 and 4 seconds.

4. X-ray Photoelectron Spectroscopy (XPS)

Surface analysis was done using X-ray photoelectron spectroscopy (XPS, Kratos AXIS Ultra spectrometer with a monochromatized Al K α source). Concentric hemisphere analyzer (CHA) was used in XPS. Both survey (10~1000 eV) and high resolution scans on carbon 1s (270~295 eV) and oxygen 1s (520~540 eV) were conducted; fitting of the curves of high resolution scans were performed using Gaussian functions. The incident angle of incoming X-ray was vertical to the sample surface which enables one to explore the chemical structure of the sample at greater depth (~10 nm).

5. Interferometry for Thermal Stability (ITS)

Thermal stability was measured using interferometry for thermal stability (ITS) apparatus described by Cruden et al.²⁹. The change in film thickness was monitored by noting the reflectance of 632.8 nm helium–neon laser beam off the substrate. The thicknesses of all films used were between 1.3~1.5 μm . In this thesis, the polymer thin films deposited on silicon wafer were kept under nitrogen atmosphere for 20 minutes in nitrogen to purge the residual oxygen inside ITS chamber right before the start of the experiment and then while the nitrogen purge continued, the temperature was ramped from room temperature in an exponential manner to 400 $^{\circ}\text{C}$ in 70 minutes in an exponential manner and was held at 400 $^{\circ}\text{C}$ for another 60 minutes. Figure 1 shows the temperature programming.

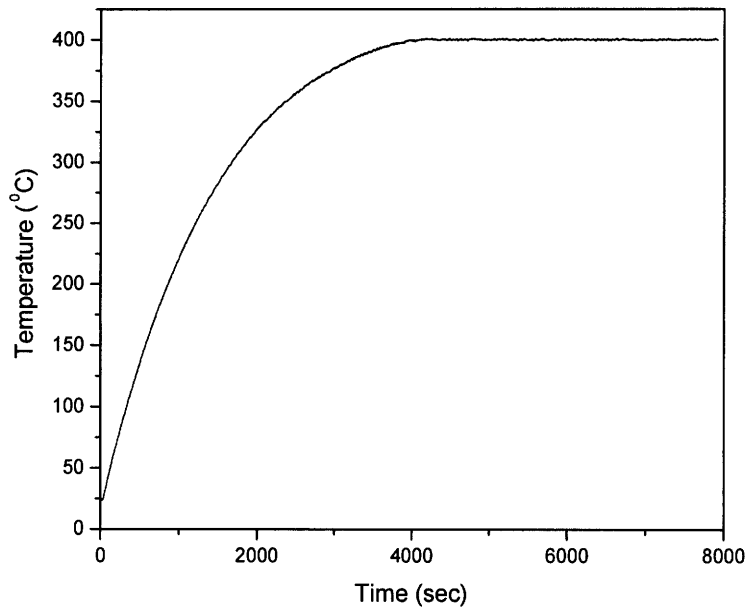
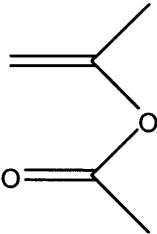
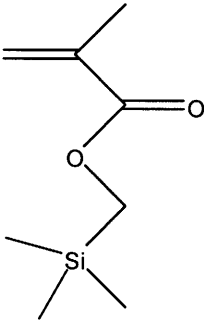
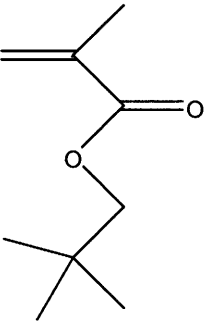
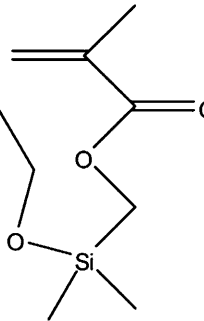
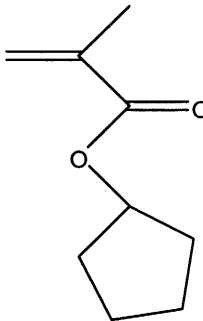
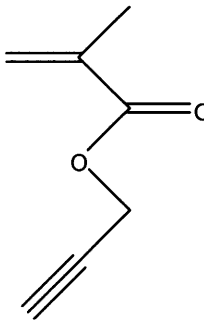


Figure 1: temperature programming in ITS experiments

6. Variable Angle Spectroscopy Ellipsometry (VASE)

Thicknesses and refractive indices of the deposited polymer thin films were determined using VASE (JA Woollam M-2000); measurements were done at three angles (65, 70 and 75 degrees) and the range of wavelength was in 315 nm to 700 nm. A Cauchy-Urbach model was used to fit

Table 2-1: Conditions of deposition of various monomers

Abbreviation	IpAc	TMMA	npMA	EMSMA	CPMA	PMA
Structure						
Vapor pressure At 25 ^o C (torr)	42.5	0.724	0.923	0.326	0.387	4.23
Total pressure (torr)	9	0.76	1.235	0.285	1.425	1.52
F _{monomer}	10	4.5	3.0	1.8	1.5	4.5
F _{TBPO}	0.5	0.5	1.0	1.0	0.5	0.5
T _{stage}	300	295	280	275	275	265
T _{filament}	25	25	25	35	30	25

the experimental results⁶.

7. Thermogravimetric analysis (TGA)

The TGA was performed using a TA Instruments TGA2950 (TA Instruments P/N 952250.502 S/N HA2950-R516). The purge atmosphere was nitrogen at 100 ml/min. The temperature program was a linear ramp at 10 °C/min to 600 °C. The samples were held in platinum TGA pans. Data collection used Thermal Advantage software v.1.1A S/N C1102272 and the analysis used Universal Analysis v. 3.4C build 3.4.0.10.

8. Flash pyrolysis – gas chromatography mass spectroscopy (FP-GCMS)

FP-GCMS experiments on P(npMA), poly(ethylene glycol diacrylate) (P(EGDA)) and P(npMA-*co*-EGDA) was performed by Dr. Jim Carnahan at Edison Analytical Laboratories, Inc. (Schenectady, NY; website: <http://www.edison-labs.com/>). Polymer sample was left overnight in a vacuum oven before pyrolysis to minimize the amount of absorbed volatile species. One to two milligrams of sample was placed on pre-cleaned aluminum sheets and rolled up, inserted into the sealed end of a 40 cm*1 cm Pyrex tube. The tube was then pumped down to vacuum and the open end was melt sealed. Half of the tube was then inserted into a furnace at desired temperature (in this study 400 °C); the other half was still in contact with ambient. The end of this half was cooled with liquid nitrogen in order to condense and collect the degraded products and prevent secondary reaction. When the pyrolysis was complete, the tube was cut in half and one milliliter of methylene chloride was added to dissolve degraded products. 1 µl of the solution was manually injected into the injection port heated at 260 °C. The temperature of GC column was kept at 40 °C for 5 minutes and ramped at 20 °C/min to 300 °C within 10 minutes. The column was 0.32 inch in diameter and coated with 1µm of poly(dimethylsiloxane). Peak identification of was via the Wiley-NIST mass spectral library and PBM search routine. GCMS experiments were also

performed on npMA and EGDA monomers in order to obtain the standard mass spectra and the reference retention time in GC columns.

The GC-MS is an HP5890 GC connected to an HP5972 mass selective detector. The GC column was a 30 meter ZB-1 with an ID of 0.32mm and a phase thickness of 1.0 microns. The temperature program was an initial isothermal hold for 5 minutes at 40 °C followed by a linear ramp at 20 °C/min to 300 °C with a 10 minute hold. The injector temperature was 260 °C and the injection mode was splitless with a purge valve open time of 1.0 min. The interface to the MSD was open split and the interface temperature was 280 °C. Peak identification was via the Wiley-NIST mass spectral library and PBM search routine.

9. Nanoindentation

Hysitron TriboIndenter[®] was used for nanoindentation on copolymer samples. Z calibration was done in air with maximal load of 700 μm to find out that the relation between the applied voltage and the resulting load. H calibration was conducted on aluminum metal to find out displacement vector between the microscope and the indenter so that the latter indents exactly where is shown under the microscope. Frame compliance of the indenter and area function of the diamond tip were determined by performing indentation on fused silica which has a known modulus of 69.6 GPa; the load of indentation was increased from 0.1 mN to 10 mN by 0.1 mN between neighboring indents. Frame compliance was calculated based on the load-displacement relation where the loads are between 5 to 10 mN and the area function was obtained by fitting the curves that have similar displacement as those values one gets from indentation experiments on polymer samples. The moduli and hardnesses were obtained by using the software accompanying the triboindenter.

Nanoindentation experiments were conducted using a conical diamond tip (Young's

modulus = 1140 GPa, Poisson ratio = 0.07) with 1 μ m curvature and the maximum loading was set to be less than 50 μ N so that the indents were always less than 10 percent of thickness of polymeric materials of interest. Indents beyond 10 percent of the thin film thickness of should be avoided due to the likely interference of the substrate; indents less than 20 nm are often complicated by noise and should be avoided as well. The loading function consists of four segments: (1) the tip barely touches the sample surface and stays there for 10 seconds, (2) the loading is gradually applied via the tip to the surface for 10 seconds without exceeding 50 μ N, (3) the tip is fixed for 10 seconds at where is it in the material and (4) the unloading takes another 10 seconds. The third segment is unique for viscoelastic polymeric materials since polymers creep even after the loading process stops and it is necessary to wait for a certain period of time so that the creeping ceases; this is not required for metal/ceramic materials. Figure 2 and 3 illustrate the typical loading-unloading curves of metal/ceramic and polymeric materials, respectively. Note the order of magnitude

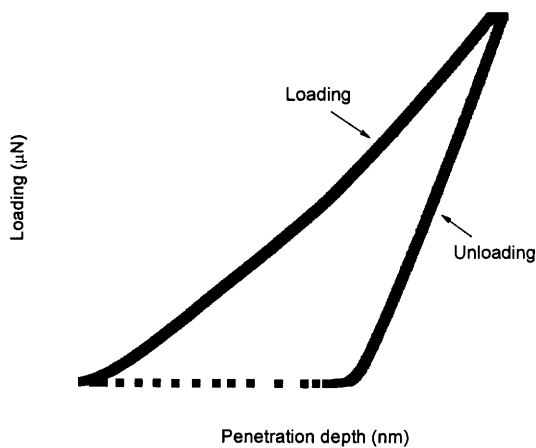


Figure 2: Typical loading and unloading curves in nanoindentation test; fused silica used as standard

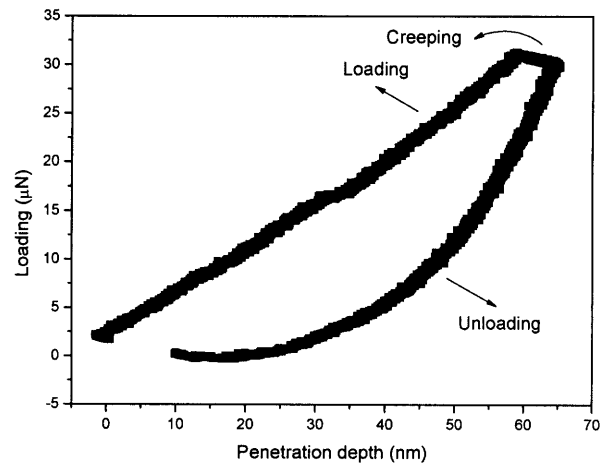


Figure 3: Nanoindentation loading-unloading curves of P(npMA-co-EGDA)

of loading on the two figures is quite different due to the much higher modulus of metal/ceramic materials.

The model developed by Oliver and Pharr²⁸ was used in the determination of Young's modulus. The slope of the loading curve is related to Young's modulus of the material under nanoindentation. In this thesis the slope from 40 to 95 percent of maximal displacement of unloading curve was calculated to extract the two mechanical properties. Fused silica ($E=69.6$ GPa) was used as standard to determine the frame compliance and area function. A 5*5 grid of indents was performed on each sample, with each indent separate from each other by 2 μm in x and y direction to meet the statistical requirement. 8192 points were taken for each indent.

10. Electron-Beam Lithography

Electron-beam lithography was used to obtain accurate size of feature on the scale of tens of nanometers. PMMA was used as positive photoresist and spincoated on the silicon wafer to which a layer of 200 ± 20 nm-thick P(npMA-co-EGDA) has been deposited. The recipe for spincoating was 500 rpm for 5 seconds and 4000 rpm for 45 seconds. This recipe was intended for 100 nm PMMA resist, high rotation speed can be applied for thinner PMMA layer if required. The spun-on wafer was heated at 180 °C for 20 minutes. The resulting thickness of PMMA was measured by VASE to be 140 nm. Raith 150 scanning e-beam lithography facility was used in e-beam direct writing at a voltage of 10 kV and a dose of 90 $\mu\text{C}/\text{cm}^2$. The dimension of feature line was 0.09 μm * 3000 μm , the spacing between two lines was 0.11 μm . After e-beam writing, the wafer was developed in the 1:2 (v/v) mixture of MIBK and IPA for 90 seconds at 21 ± 0.5 °C and immediately rinsed with IPA for 60 seconds then dried with nitrogen flow for 60 seconds.

11. Reactive Ion Etching (RIE)

The pattern generated by e-beam lithography was transferred to P(npMA-co-EGDA) layer by RIE. Oxygen was used as etchant. The flowrate, pressure and RF power were 30 sccm,

40 mtorr and 250W, respectively. RIE was performed separately on the wafers deposited with PMMA resist and P(npMA-co-EGDA) to calculate their respective etch rates to determine the thickness and time required for complete removal of PMMA layer and minimal damage to P(npMA-co-EGDA) layer.

12. Plasma-Enhanced Chemical Vapor Deposition (PECVD)

Silicon dioxide was deposited on top of the selected blanket and patterned copolymer thin films using PECVD. The flowrates of silane (5% SiH₄ in He) and nitrous oxide (N₂O) were controlled at 195±3 and 600±5 sccm, respectively, and mixed in the deposition chamber. The stage on which the silicon substrate sits was maintained at 250 °C; the power of radio frequency and the pressure in the chamber was controlled at 25W and 500 mtorr, respectively. The deposition rate was approximately 35 nm/min based on these reaction conditions.

13. Brunauer-Emmett-Teller isotherm analyzer (BET)

The porosity of silica overlayer was checked by BET surface area and porosity analyzer (Micrometrics, ASAP 2020). A piece of 4-inch bare silicon wafer was weighted and deposited with a layer of porous silica of approximate one micron in thickness by PECVD; the weight of silica layer was calculated by subtracting the weight of bare silicon wafer from the deposited one. The wafer was cut into strips, fit in the sample tube, degassed and refilled by nitrogen gas of high purity. The sample tube was then connected to analysis stage and pumped down to 0.01mtorr and simultaneously cooled down by liquid nitrogen. After stabilization of the temperature and the pressure in the sample tube, nitrogen gas was injected into the sample tube at different partial pressures. BET plot then revealed the monolayer absorbed quantity and BET constant, on which the calculation of specific surface area and pore volume are based.

Macropatterning of sacrificial polymer layer was achieved by applying 3M sticky tape to 4” silicon wafer as mechanical mask. A ten by ten grid was created by placing sticky tape, 3 to 4 mm in width and sufficiently long to cover the diameter of the wafer. The length and the width of the grid were both 3 to 4 mm. Upon completion of the mask, sacrificial layer was deposited (npMA 1.0sccm, TBPO 0.7sccm, EGDA 0.45sccm, filament and stage temperatures are 280 °C and 30 °C, respectively, chamber pressure 380 mtorr). The patterned layer was left under 5 mtorr vacuum overnight for complete desorption of volatile species such as monomers or very low oligomers. Deposition conditions of silica by PECVD were the same as described in previous section.

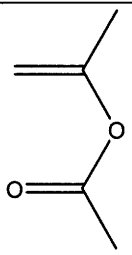
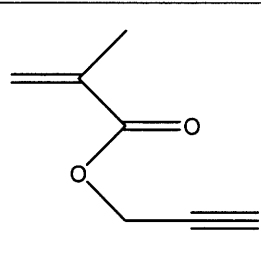
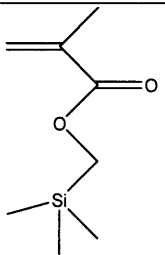
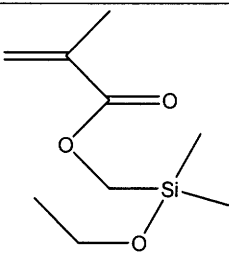
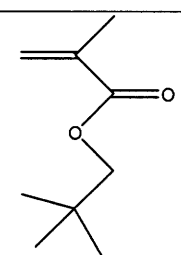
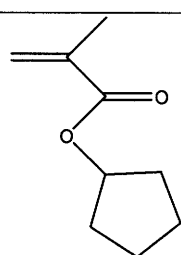
Thermal properties of homopolymer of selected mono-functional monomer

Table 2-2 shows the six monofunctional methacrylate monomers used to deposit iCVD homopolymer films for an initial screening of the thermal stability of the resultant polymers. Trimethylsilyl methacrylate (TMA), trimethylsilylmethyl methacrylate (TMMA), neopentyl methacrylate (npMA) and cyclopentyl methacrylate (CPMA) are the candidates for monofunctional component for the dual monomer approach. Ethoxydimethylsilylmethyl methacrylate (EMSMA) and propargyl methacrylate (PMA) are the candidates for the single-monomer strategy. Table 2-2 also shows the percentages of residue and the onset temperatures of decomposition (T_d) for each homopolymer; determination of T_d will be elaborated in the section of “**Interferometry thermal stability (ITS) characterization of polymer thin films on substrates**”. P(TMA) quickly hydrolyzes in ambient to form PMAA and therefore is not suitable as air-gap sacrificial material as discussed in the introduction. The T_d 's for the rest of the polymers are low compared to the results reported in literature using bulk samples in thermogravimetric (TGA) experiment.

The degradation temperature of polymer in TGA is usually determined to be the temperature where

the sample loses 5~10% of its original weight³⁹⁻⁴¹. In TGA experiments, the degradation temperature is polymethacrylates generally between 200 to 250 °C, depending on the heating profile^{14,39,42}. The discrepancy in onset temperature of decomposition obtained from ITS and TGA experiments may be attributed to the low molecular weights of the iCVD films. For example, the weight-averaged molecular weight of P(TMMA) is about 19,700 Da and the polydispersity index (PDI) is about 1.45, implying the likely adsorption or retention of volatile monomers and oligomers on polymer surfaces or within polymer matrices, respectively. Another potential factor is that the samples are deposited onto a substrate as a thin film, thus exposing more free chain ends than a bulk sample.

Table 2-2: Onset temperatures of degradation of thin films deposited on silicon wafer (T_d) and removal percentages of homopolymers consisting of selected monomer

Monomer	IpAc	PMA	TMMA	EMSMA
Structure				
T_d (C)	140	100	115	115
Removal percent After 400C for 1hr	~100	~80	~100	~97.7
Monomer	npMA		CPMA	
Structure		M.W.: 156.22Da B.P.(1 atm): 179.8C V.P. (25C): 0.923torr Hazard: Flammable		M.W.: 154.21 Da B.P. (1 atm): 197.0C V.P. (25C): 0.387torr Hazard: Flammable
T_d (C)	135		120	
Removal percent after 400C for 1hr	~100		~100	

The P(PMA) and P(EMSMA) are not observed to decompose cleanly. One possible explanation is that some of the PMA monomers become dimers during the short contact time with the hot filament which contains copper metal and possibly copper (I)²³⁻²⁴ due to heating, exposure to air and interaction with monomers. Oxidative addition of monosubstituted acetylene to copper (I) has been reported in numerous publications, and the two acetylene groups bonded to copper (I) are coupled to form diacetylene and eventually cleaved via reductive elimination. Upon heating, diacetylene groups form various types of crosslinkers, enhancing the thermal stability²³⁻²⁴. For P(MSMA), the condensation of the ethoxy groups of EMSMA and silanol group on wafer surface is likely to cause incomplete removal of polymers since the siloxane bonds are very strong.

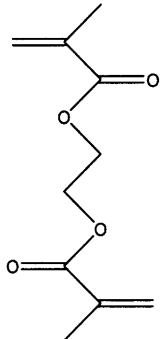
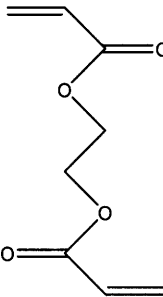
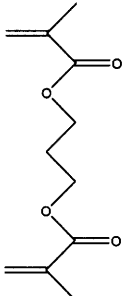
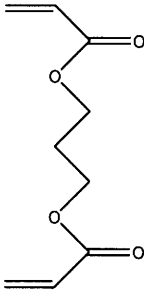
The results of the first experimental screening step therefore limit the pool of selection of monomers to TMMA, npMA and CPMA, all candidates for the two-monomer strategy. This indicates the need to incorporate crosslinkers to increase the thermal stability. TMMA were not chosen for final two candidates based on its lower thermal stability and the larger size compared to npMA and CPMA.

Thermal properties of homopolymer of selected bifunctional monomer

Table 3 shows the four crosslinkers of interest in the present research: ethylene glycol dimethacrylate (EGDMA), ethylene glycol diacrylate (EGDA), 1,3-propanediol dimethacrylate (PDDMA) and 1,3-propanediol diacrylate (PDDA). EGDMA and EGDA have two methylene groups between the polymerizable groups as spacer while PDDMA and PDDA have three. Table 4 shows the onset temperatures of degradation and the removal percentages of homopolymers of crosslinkers. As expected, the onset temperatures of thermal degradation (T_d) of homopolymers of crosslinkers are much higher than those of the monofunctional vinyl monomers shown in Table 1. It is apparent that P(EGDMA) and P(PDDMA) decomposed quite cleanly but the T_d of P(PDDMA) is

much lower than that of P(EGDMA). Analogously, T_d of P(PDDA) is lower than that of P(EGDA). P(EGDA) and P(PDDA) decompose less cleanly than their dimethacrylate counterparts, leaving 7–8 percent of residue. It is speculated that longer distance between crosslinking points facilitates the thermal motion of polymer chain segments and therefore lowers the T_d . Based on the removal

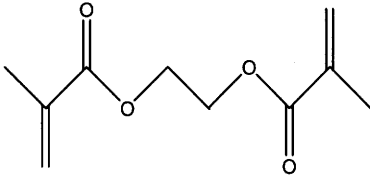
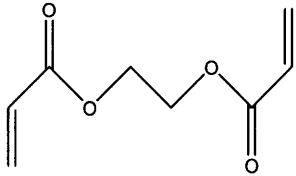
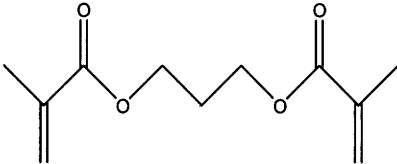
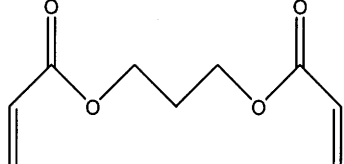
Table 3: Potential candidates of crosslinkers

Ethylene glycol dimethacrylate (EGDMA)		Ethylene glycol diacrylate (EGDA)	
	<p>M.W.: 198.22 Da</p> <p>B.P. (at 760mmHg): 260~261 °C</p> <p>Vapor pressure (25C): 12.1 mtorr</p>		<p>M.W.: 170.16 Da</p> <p>B.P. (at 760mmHg): 223.9±13.0 °C</p> <p>Vapor pressure (25C): 93.9 mtorr</p>
1,3-propanediol dimethacrylate (PDDMA)		1,3-propanediol diacrylate (PDDA)	
	<p>M.W.: 212.25 Da</p> <p>B.P. (at 760mmHg): 278.7±13.0 °C</p> <p>Vapor pressure (25C): 4.21 mtorr</p>		<p>M.W.: 184.19 Da</p> <p>B.P. (at 760mmHg): 243.1±13.0 °C</p> <p>Vapor pressure (25C): 32.7 mtorr</p>

percentage and T_d , EGDMA and EGDA were selected for further research involving copolymerization with npMA and CPMA. Note that EGDMA and EGDA do have beta-hydrogens and theoretically they can be abstracted by ester oxygen to form acid group and eventually neighboring acid groups form very thermally stable anhydrides, which reduce the removal percentage substantially. However the removal percentages were almost 100% and 92% for P(EGDMA) and P(EGDA), respectively, implying beta-hydrogen abstraction does not play a

significant role in thermal degradation of the present system and decomposition conditions. This result suggests that intensive crosslinking limits chain movement and helps prevent beta-hydrogen abstraction from occurring.

Table 4: Onset temperatures of degradation of thin films deposited on silicon wafer (T_d) and removal percentages of homopolymers consisting of selected crosslinkers

Crosslinker	EGDMA	EGDA
Structure		
T_d (C)	300	350~375
Removal percent (%)	99.52±0.27	92.12±0.25
Crosslinker	PDDMA	PDDA
Structure		
T_d (C)	235	300~325
Removal percent (%)	99.46±0.11	93.15±0.43

Copolymerization of selected monomers and crosslinkers

Table 5 lists the deposition rate, the onset temperature of degradation (T_d) and the removal percentage after heating at 400 °C for an hour under nitrogen atmosphere for the each of the four combinations from monomers (npMA and CPMA) and crosslinkers (EGDMA and EGDA).

P(npMA-*co*-EGDMA) and P(CPMA-*co*-EGDMA) systems decomposed cleanly but the T_d 's were low compared to P(npMA-*co*-EGDA) and P(CPMA-*co*-EGDA). Increasing the amount of EGDMA in P(npMA-*co*-EGDMA) and P(CPMA-*co*-EGDMA) systems would certainly improve the thermal

stability but the upper limit of such methodology will not surpass 300 °C, the T_d of P(EGDMA) shown in Table 4. On the other hand, despite of the fact that the copolymers of P(npMA-co-EGDA) and P(CPMA-co-EGDA) did not decompose as cleanly as the systems where EGDMA was used as the crosslinker component, the amount of residue would reduce with increasing amount of methacrylate monomers and therefore EGDA was chosen as the crosslinker component. As for the selection of monomer component, npMA demonstrated superior deposition rate, T_d and removal percentage to CPMA and therefore made it the better option in sacrificial materials.

Table 5: Onset temperature of thermal degradation, removal percentage and deposition rate of selected copolymers

Copolymer	P(npMA-co-EGDMA)	P(CPMA-co-EGDMA)
Deposition rate (nm/min)	61.5	63.0
T_d (C)	230~240	240
Removal percent (%) after 400C for 1hr	99.58±0.01	99.57±0.26
Copolymer	P(npMA-co-EGDA)	P(CPMA-co-EGDA)
Deposition rate (nm/min)	88.7	51.4
T_d (C)	330	280~290
Removal percent (%) after 400C for 1hr	95.56±0.25	90.74±0.48

As monomers, npMA and CPMA have approximately the same molecular weight (npMA: 156.22Da, CPMA: 154.21Da), dimension (npMA: 10.13 Å * 5.20 Å * 5.30 Å; CPMA: 9.43 Å * 5.93 Å * 4.88 Å), as simulated by Gaussian Software and shown in Figure 4 and vapor pressure (npMA: 0.923 torr, CPMA: 0.387 torr, calculated at 25 °C) ³⁰. The major differences lie in the structures of side groups, namely neopentyl and cyclopentyl moieties. During polymerization, the

presence of cyclopentyl groups in the closer proximity to the radical center constitutes higher steric hindrance compared to that of neopentyl groups and results in lower polymerization as well as deposition rates of homopolymer and copolymer. Indeed, at identical conditions, a lower deposition rate of P(CPMA) was observed (20 nm/min) compared to that of P(npMA) (30 nm/min). The availability of beta-hydrogen on cyclopentyl groups is unlikely to contribute to the lower removal percentage of P(CPMA-*co*-EGDA) since the beta hydrogens on alicyclic structure are much farther away (~ 2.5 Å) from ester oxygen compared to linear aliphatic side groups (~ 2.0 Å) such as in poly(n-pentyl methacrylate); the decomposition of P(CPMA) was also complete under the same thermal annealing conditions for P(npMA) which confirms that beta-hydrogen abstraction was not a major issue. Detailed studies are required to explain the differences in T_d and removal percentage between P(npMA-*co*-EGDA) and P(CPMA-*co*-EGDA).

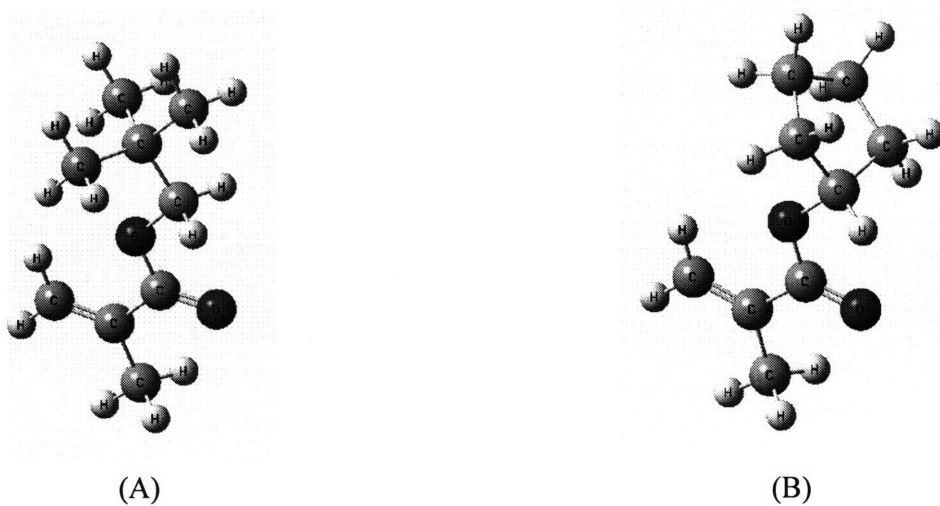


Figure 4: Optimized structure of (A) npMA and (B) CPMA monomer

Characterization of P(npMA-co-EGDA)

P(npMA-co-EGDA) was selected as the model for detailed study for sacrificial material application based on the suitable thermal stability, high deposition rate and the potential of improving the removal percentage by increasing the methacrylate monomer content. Spectroscopic features, chemical/solvent resistance, thermal stability and degradation rates and mechanical properties of the copolymer were investigated on copolymers having different compositions in order to understand the relation between the compositions and the properties and eventually optimize the performance.

Fourier transform infrared (FTIR) IR spectra of P(npMA-co-EGDA) and curve fitting of characteristic peaks

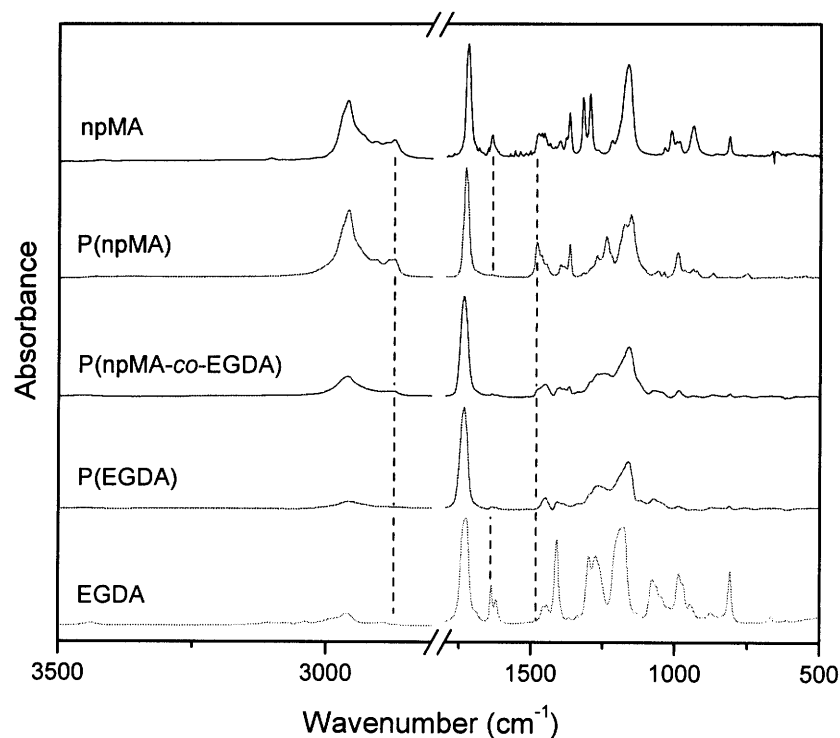


Figure 5: FTIR spectra of monomer and homopolymer of npMA and EGDA and copolymer thereof

Figure 5 shows the IR spectra of npMA and EGDA monomers, their homopolymers as well as one

of the copolymers with $F_{npMA} = 1.0$ sccm. The peak of medium intensity at 1640 cm^{-1} is characteristic of carbon-carbon double bonds for methacrylate monomers. The doublet peaks at 1635 cm^{-1} and 1620 cm^{-1} are characteristic of acrylic monomers due to symmetric and asymmetric stretching of carbon-carbon double bonds. Upon polymerization these peaks disappear, indicating the complete consumption of vinyl bonds and confirming the feasibility of iCVD methodology. The FTIR spectrum of P(EGDA) shows peak of very low intensity at the position characteristic of carbon-carbon double bond stretching, suggesting the presence of a small percentage of polymerizable groups in the polymer, as well as the homopolymers of other crosslinkers (FTIR not shown). This is quite common in polymerization of multi-functional monomers; polymerizable groups not consumed at the initial stage of polymerization tend to survive as the reaction proceeds due to decreasing mobility of the polymer matrix. The peak around 1730 cm^{-1} is the stretching of carbonyl group. The carbonyl stretching modes at 1721 cm^{-1} for npMA, 1728 cm^{-1} for P(npMA) and EGDA and 1735 cm^{-1} for P(EGDA). The peak at 2870 cm^{-1} is indicative of the methyl groups on neopentyl moieties of npMA and P(npMA) but is not observed for EGDA and its homopolymer which both lack of methyl groups. The peaks at 1480 cm^{-1} and 1450 cm^{-1} are C-H bending modes for npMA²⁵ and EGDA, respectively, and these peaks do not show appreciable shift in the respective polymers as illustrated in figure 4. Both 1480 cm^{-1} and 1450 cm^{-1} were observed in the FTIR spectrum of P(npMA-co-EGDA) copolymer with attenuated intensities. Figure 6 shows the FTIR spectra of commercial P(npMA) spun-cast film and the iCVD-synthesized P(npMA). The commercial sample was synthesized via conventional free-radical polymerization pathway. The peak positions and relative intensities of the iCVD P(npMA) are essentially the same as commercial ones as shown in Figure 6 and confirms that polymerization of npMA by iCVD methodology resulted in the same product. Figure 7 shows the systematic change in the intensities of these peaks in accordance with the increase in the flowrate of npMA. As the flowrate of npMA increased, the intensity of 1480 cm^{-1} peak increased accordingly.

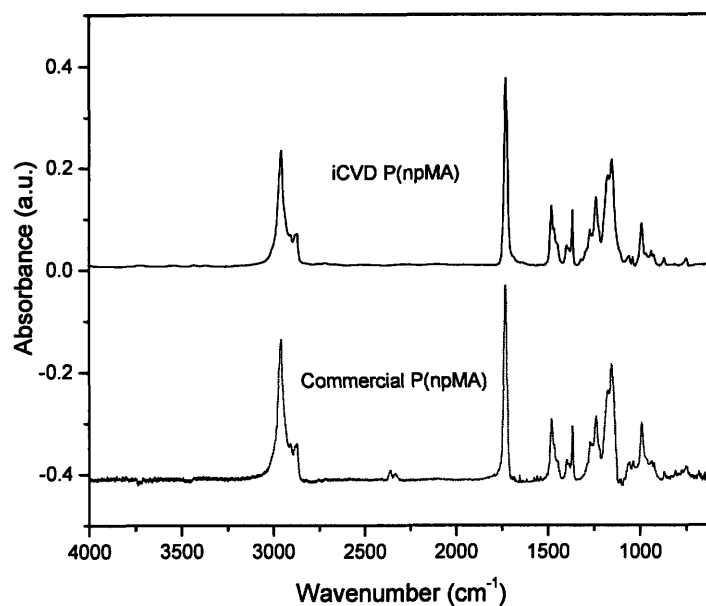


Figure 6: Comparison of iCVD and commercial P(npMA) polymerized via free radical pathway

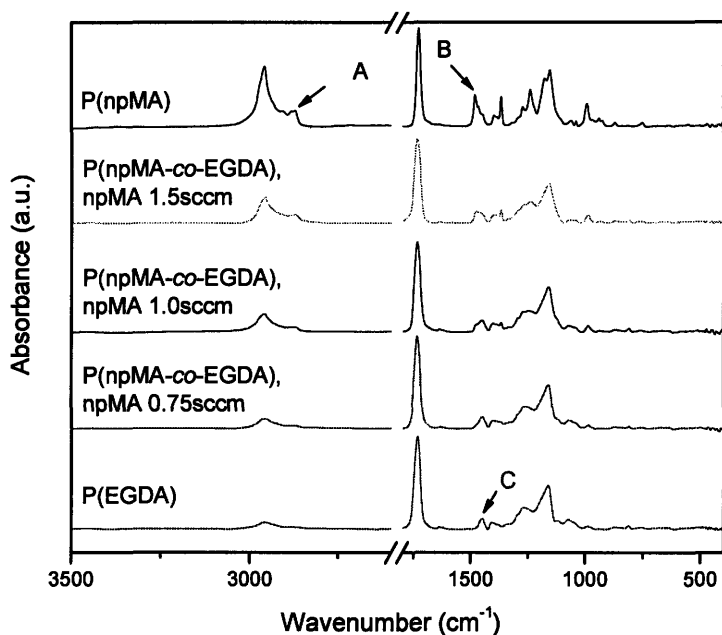


Figure 7: FTIR spectra of P(npMA-co-EGDA) copolymer

Curve fitting of characteristic peaks of npMA and EGDA was attempted to determine the bulk composition of the copolymer thin film by using the peaks at 2870 cm^{-1} , which is characteristic of npMA moieties, and the carbonyl group. However the attempt was not successful due to the difficulty of resolving the overlapping peak in region of carbon-hydrogen bond stretching after

polymerization.

Nuclear Magnetic Resonance spectra of P(npMA)

Figure 8 shows the ^1H NMR spectra of npMA and P(npMA) (the exact iCVD conditions for the growth of P(npMA) is described in Table 2-1) with the peak assignments designated to specific protons. The peak assignment (chemical shift in ppm): (1) npMA: 6.14 (1H, quintet, proton trans to carbonyl), 5.57 (1H, quintet, proton cis to carbonyl), 3.85 (2H, singlet, $-\text{COOCH}_2\text{C}(\text{CH}_3)_3$), 1.98 (3H, triplet, protons on vinyl methyl) and 0.99 (9H, singlet, $\text{COOCH}_2\text{C}(\text{CH}_3)_3$). (2) P(npMA): 3.50~3.80 (2H, multiple, $-\text{COOCH}_2\text{C}(\text{CH}_3)_3$), 1.86~2.10 (2H, protons on methylene groups on polymer backbone) and 0.85~1.15 (12H, protons on methyl groups).

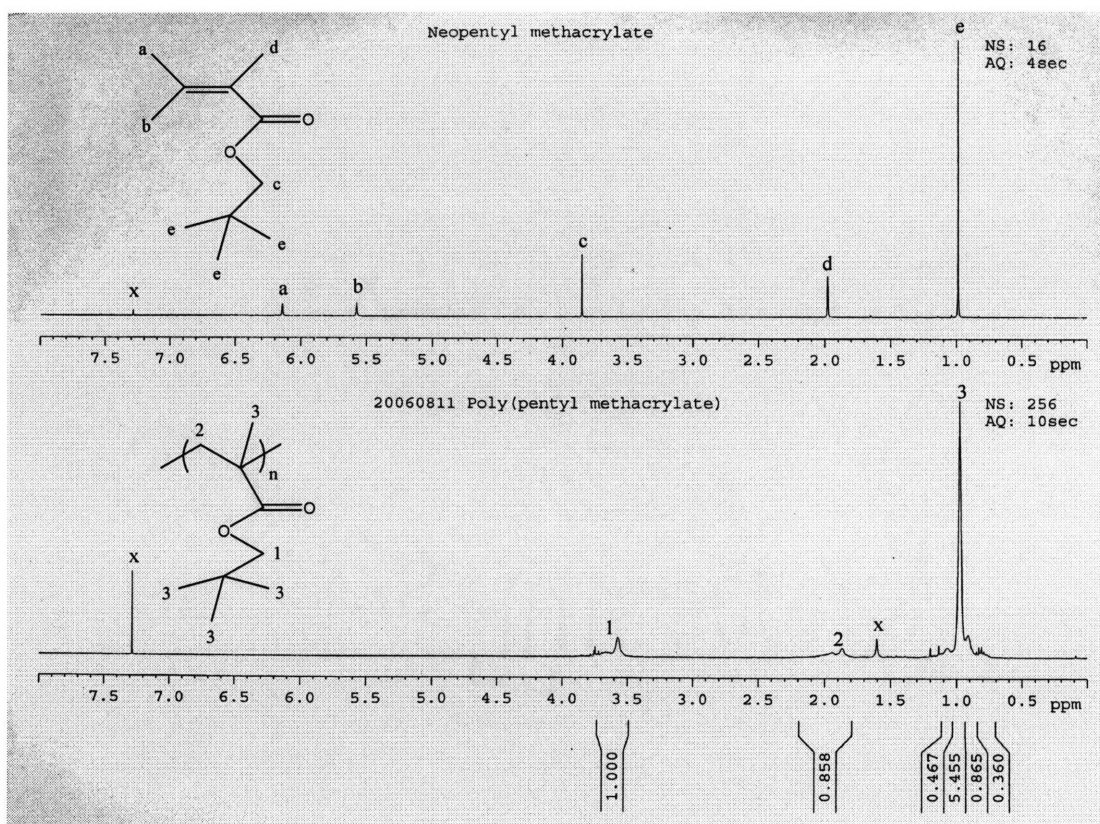


Figure 8: ^1H NMR of npMA and Poly(npMA); CDCl_3 used as deuterated solvent.

It is clear that vinyl proton peaks at 5.57 and 6.14 ppm are present only in the monomer, confirming

that vinyl polymerization is the mechanism by which the iCVD polymer films are produced. The protons on the methylene group next to ester oxygen were at 3.85 ppm in the npMA proton NMR spectrum but shifted to 3.57 ppm and broadened after polymerization. The peak broadening in NMR is related to conformation of polymer chains in solution state⁴³. The protons on methyl group next to the double bond shifted from 1.98 to the range of 0.85~1.15 ppm^{25, 44}. The ratio of integrated peak areas in proton NMR of P(npMA) showed that the neopentyl side groups remained intact during iCVD process; the ratio of peak area at 3.85 and 0.99 ppm was 2:9 in proton NMR spectrum of npMA as expected. In the proton NMR spectrum of P(npMA), the ratio of peak area at 3.57 and 0.08 ppm was 2:12. Subtracting the contribution from the methyl group on the polymer backbone the ratio of 2:9 was recovered which implied that neopentyl group is retained. The ratio of integrated peak area for iCVD P(npMA) was 1:0.85:6.25; the ratio did not change by increasing the acquisition time from 2 second to 10 second. The proton NMR of commercial P(npMA) also showed three broad clusters of peaks with very similar distribution in signal intensities at 3.50~3.70 ppm, 1.75~2.10 ppm and 0.80~1.20 ppm with the integrated peak ratio of 1:0.8:6, which was essentially the same ratio as that of iCVD P(npMA). This again confirmed that validity of iCVD methodology. Liquid state NMR are extremely difficult for P(EGDA) and P(npMA-co-EGDA) since they are highly crosslinked and do not readily dissolve in any common solvent. Nevertheless, it is expected that the EDGA moieties stayed unchanged since they are more thermally stable and the dimethylene bridge connecting the two polymerizable functional groups are also saturated hydrocarbon segments.

XPS of deposited thin film: P(npMA), P(EGDA) and P(npMA-co-EGDA)

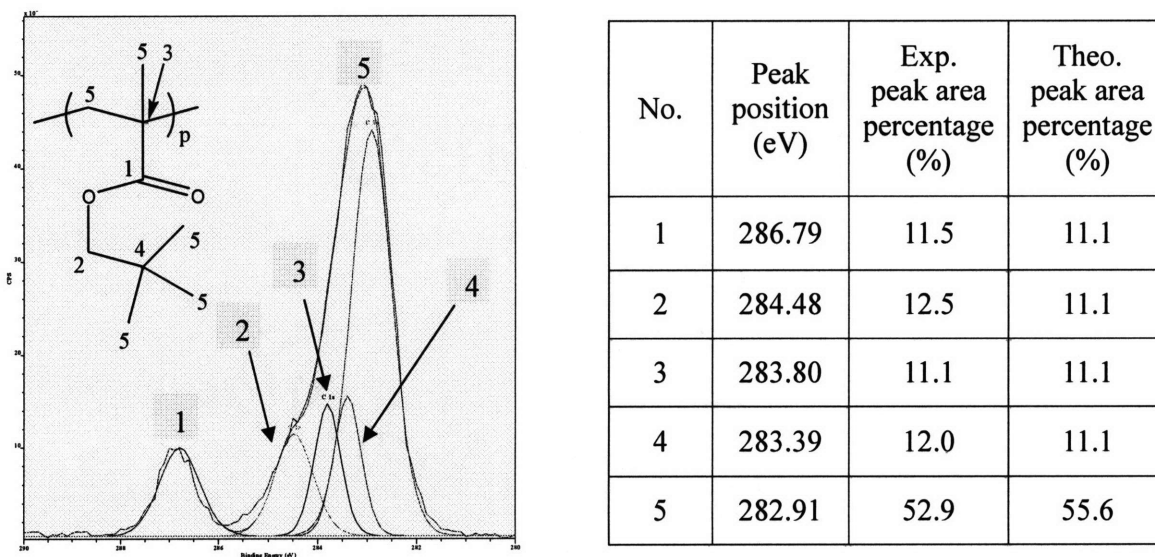


Figure 9: XPS diagram and curve fitting result on P(npMA)

The C1s high resolution scans are shown in figure 9 and 10 for P(npMA) and P(EGDA), respectively. Five distinct peaks in the P(npMA) spectra were found and the ratio of peak areas was approximately 1:1:1:1:5, which, in order of increasing/decreasing binding energy corresponds to carbonyl carbon (286.79eV), sp^3 -carbon bonded to ester oxygen (284.48 eV), quaternary carbon on the polymer backbone (283.80 eV), quaternary carbon on the side group (283.39 eV) and the rest of the carbon atoms on the polymer backbone and side group (282.91 eV). In figure 10, three bonding environments were distinguished and corresponded to the carbonyl group (287.30 eV), the sp^3 -carbon atom bonded to ester oxygen (285.08 eV) and the backbone carbon atoms of P(EGDA) (283.56 eV), in the expected ratio of peak area of 1:1:2.

The O1s high resolution scan of P(npMA) and P(EGDA) are shown in the left-hand side inset in figure 11. Both scans have two peaks of approximately the same area, implying there are two distinct types of oxygen atoms corresponding to the carbonyl and ester groups. Exploration of the chemical structures of P(npMA) and P(EGDA) at greater depth (~10 nm) was made possible by the vertical incident angle of X-ray and both the C1s and O1s scans confirm the expected polymer

chemical structure.

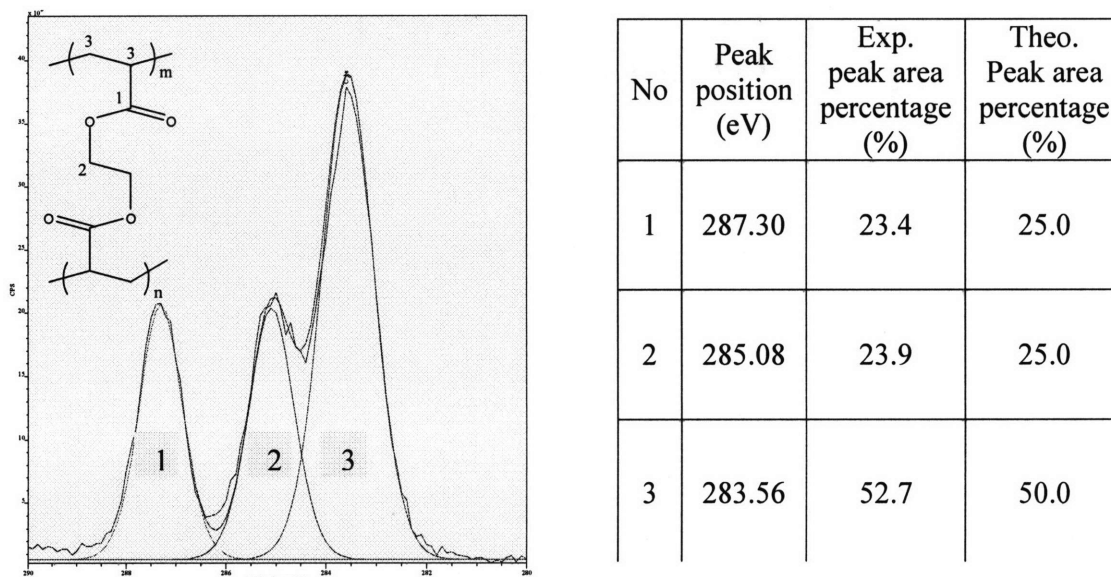


Figure 10: XPS diagram and curve fitting result on P(EGDA)

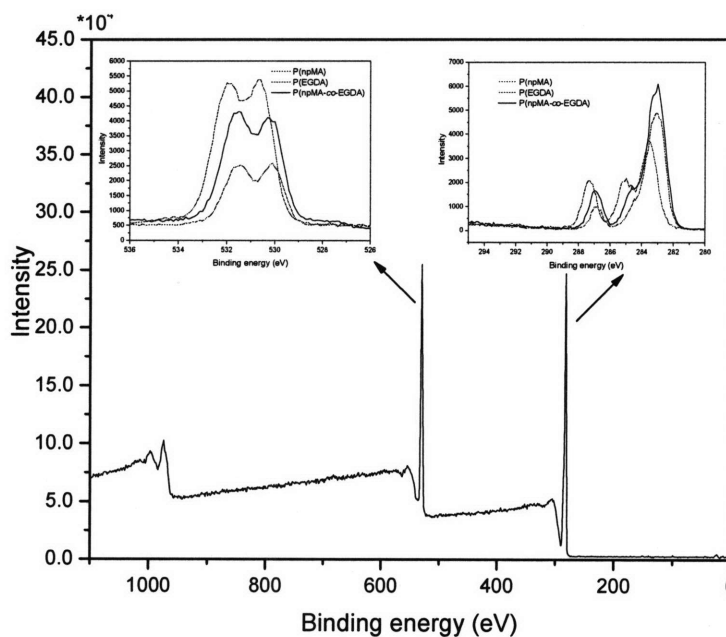


Figure 11: XPS scan on carbon and oxygen of P(npMA-co-EGDA), $F_{npMA} = 1.0$ sccm

The survey and high resolution scan of P(npMA-co-EGDA) with $F_{npMA} = 1.0$ sccm are shown in figure 11, the higher resolution scans of P(npMA) and P(EGDA) are given for comparison. The survey scan shows that only carbon and oxygen atoms were present. Comparison with the results of

homopolymers revealed that XPS curve of copolymer contains both the feature of P(npMA) and P(EGDA). For example, both the peaks of methyl groups on P(npMA) (282.91 eV) and the methylene groups on P(EGDA) (283.56 eV). Table 7 shows the ratio of total peak area of carbon (C1s), $Area_{carbon}$, and oxygen (O1s), $Area_{oxygen}$, for five P(npMA-co-EGDA) copolymers in XPS high resolution scan. The values for P(npMA) and P(EGDA) were listed for reference. The total peak areas were calculated by numerical integration.

The ratio of number of carbon and oxygen atoms present on the sample surface were obtained by the following expression:

$$\frac{\frac{Area_{carbon}}{S.F._{carbon}}}{\frac{Area_{oxygen}}{S.F._{oxygen}}} = R(C : O) \text{---(Eqn. 1)}$$

where S.F. stands for sensitivity factor. The sensitivity factor for carbon and oxygen atoms were calibrated based on the theoretical values for R(C:O) for pure bulk P(npMA) and P(EGDA) of 4.5 and 2, respectively. However it is important to note that XPS is a surface characterization technique and 95 percent of the electrons excited by incident X-ray emanate within three times of inelastic mean free path, which is only a few nanometers³⁷. A higher ratio of number of atoms of carbon to oxygen than theoretical value at the surface is possible, since the groups with low surface energy tend to segregate near the air-sample interface to minimize the energy. Since neopentyl groups are lower in surface energy compared to carbonyl groups or ester linkages it is more likely for them to tend to aggregate near the surface and as a result cause the number of “detected” carbon atoms to increase compared to oxygen atoms. Despite that caveat the surface may be carbon rich compared to the bulk film, the experimentally measured ratio R(C:O) consistently increases as expected with increasing F_{npMA} used during the deposition.

Table 7: Ratio of total peak area of carbon (C1s) and oxygen (O1s) in high resolution scan in XPS

	P(EGDA)	0.75	1.0	1.25	1.5	1.75	P(npMA)
Area _{carbon} (A _C)	5527.5	5070.6	4941.2	4850	5436.2	5330.4	3884.9
Area _{oxygen} (A _O)	4395.4	3606.1	2673.1	2549.9	2782.3	2646.8	1458.3
A _C /A _O	1.257	1.406	1.849	1.902	1.954	2.014	2.664
(A _C /S _C)/(A _O /S _O)	3.32	3.71	4.88	5.02	5.16	5.31	7.03
Theo. (#C/#O)	2						4.5
%EGDA	100	80.9	40.8	37.1	33.7	30.2	0

Interferometry thermal stability (ITS) characterization of polymer thin films on substrates

Typical ITS response curves during thermal degradation of polymer thin films shown in Figure 12 and 13 are the interferometry laser signal recorded with respect to temperature and time, respectively. The heating rate used is detailed in the experimental section. In figure 12, the interferometry signal remained at approximately the same value until fluctuation with constant amplitude occurred, which is indicative of thermal decomposition due to change in the thickness of the thin film. The local fluctuations of signal were caused by the instability of the signal recorder and were on the order of 0.1 unit on the ordinate and essentially did not significantly affect the analysis. The temperature at the intersection of two curves, one lying on the straight line of constant interferometry signal and the other tangent to the first half cycle with constant and large variation in signal, was assigned the onset temperature of thermal degradation (T_d), as shown in figure 12.

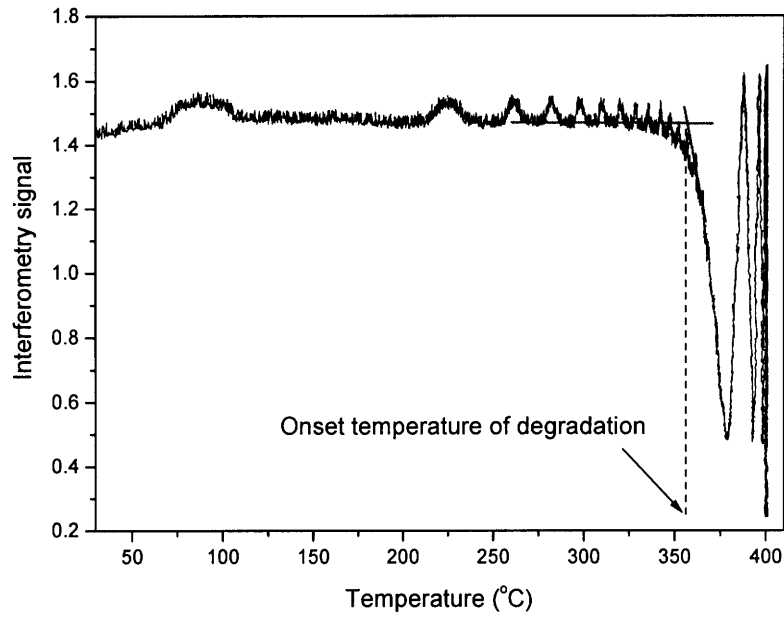


Figure 12: Typical ITS diagram and the determination of onset temperature of degradation

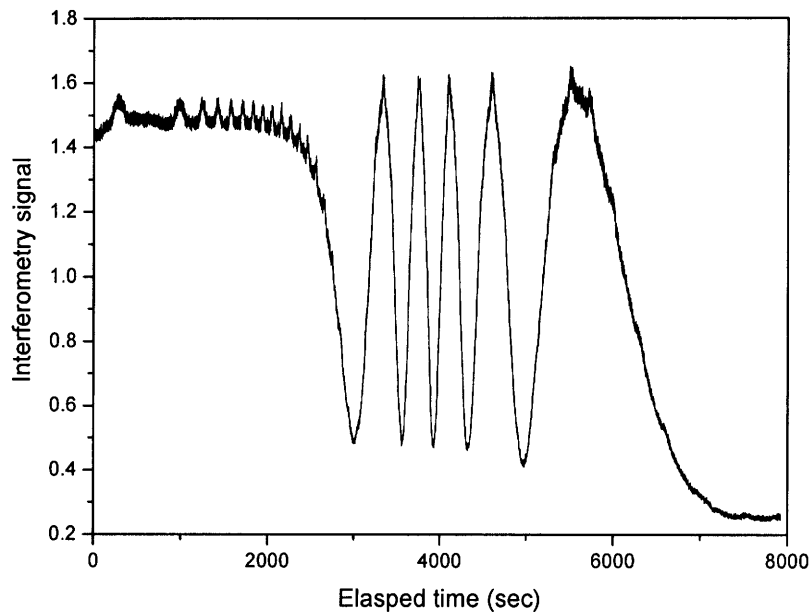


Figure 13: Variation of interferometry signal (and thus thickness) with time

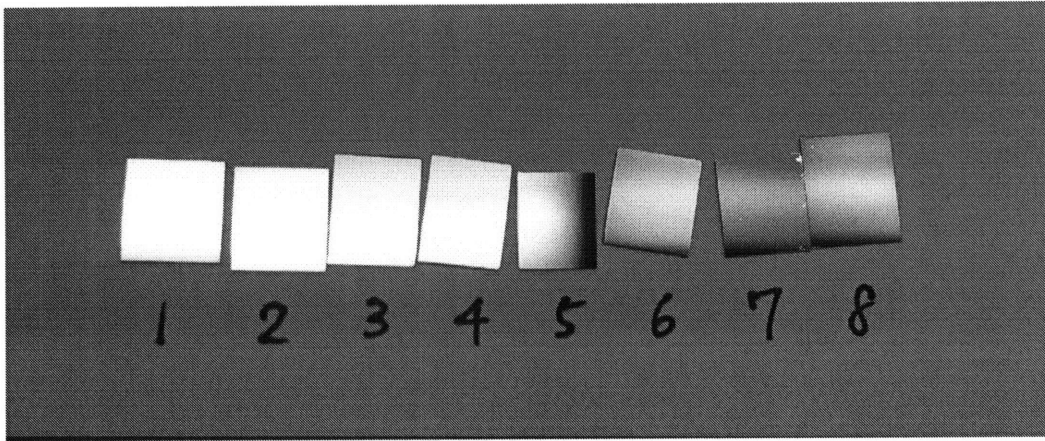


Figure 14: Photograph of polymer samples deposited on silicon wafer after ITS test: (1) Bare silicon wafer, (2) P(npMA), (3) P(npMA-*co*-EGDA), $F_{npMA}=1.75\text{sccm}$, (4) P(npMA-*co*-EGDA), $F_{npMA}=1.5\text{sccm}$, (5) P(npMA-*co*-EGDA), $F_{npMA}=1.25\text{sccm}$, (6) P(npMA-*co*-EGDA), $F_{npMA}=1.0\text{sccm}$, (7) P(npMA-*co*-EGDA), $F_{npMA}=0.75\text{sccm}$, (8) P(EGDA)

If the thermal decomposition is complete and negligible amount of residue is left on the silicon wafer, the final signal will approximately be 1.6, which is the same value of bare silicon wafer. Figure 13 is typical when there is residue on the substrate. Figure 14 shows the picture of thermally annealed samples of homopolymers of P(npMA) and P(EGDA) as well as their copolymers with various compositions. It is apparent that as the percentage of EGDA in the thin film increased, larger amount of residue was left.

Onset temperature on decomposition and calculation of removal percentage

The thicknesses of P(npMA-*co*-EGDA) copolymer thin films before and after ITS experiments were measured by ellipsometry in the range of 315 to 700 nm. The original thickness of all samples was controlled at 1350 ± 50 nm during the iCVD process. The removal percentage was calculated by dividing the difference in thicknesses before and after ITS experiments by the original thickness and then multiplying by 100. Table 8 lists the onset temperature of decomposition and the removal percentage for five copolymer films.

Table 8: Onset temperature of decomposition and removal percentage after heating at 400C for 1 hr

Flowrate of npMA (sccm)	0.75	1.0	1.25	1.5	1.75
Onset temperature of degradation ($^{\circ}$ C)	~350	~330	~300	~300	~290
Removal percentage (%)	93.59 \pm 0.23	95.56 \pm 0.25	97.12 \pm 0.06	97.17 \pm 0.01	97.88 \pm 1.06
Controlled variables	<ul style="list-style-type: none"> Flowrate of TBPO: 0.5 sccm; flowrate of EGDA: need to calculate (3 turns of needle valve); stage temp.: 30C; filament temp.: 280$^{\circ}$C, total pressure: 760 mtorr; film thickness: ~1.3μm 				

Increasing the EGDA flowrate used for copolymer deposition was observed to enhance the thermal stability but simultaneously reduced the removal percentage of the resultant films. The generation of secondary radicals, an intermediate if EGDA follows the monomer-unzipping mechanism, is energetically unfavorable compared to methacrylate monomers because of the reduced ability of delocalizing a radical center for acrylates but acrylates will eventually unzip under more rigorous conditions. However under these annealing conditions, other chemical bonds in polymers are also likely to rupture and therefore the thermal products of polyacrylates consist of fragments, monomers and oligomers. The extensive crosslinks and the random arrangement of npMA and EGDA moieties also prevents the unzipping of the former in that segmental motion is severely retarded and the generation and propagation of radicals are suppressed. Therefore the copolymer thin film became more thermally stable as the amount of EGDA increases. It has been reported¹ that during thermal decomposition of polyacrylates, volatile species such as carbon monoxide, carbon dioxide, water, alcohols, small aliphatic and aromatic hydrocarbons were observed and the residue

contained substances of fused aromatic rings and their derivatives that were difficult to remove, which explains the increased amount of residue on substrates as more EGDA crosslinkers incorporated into the thin film. Figure 15 show the systematic variation of onset temperature of decomposition and removal percentage as the flowrate of npMA increases; P(EGDA) was also included as a reference datapoint.

Kinetic data of thermal decomposition: removal rate and activation energy

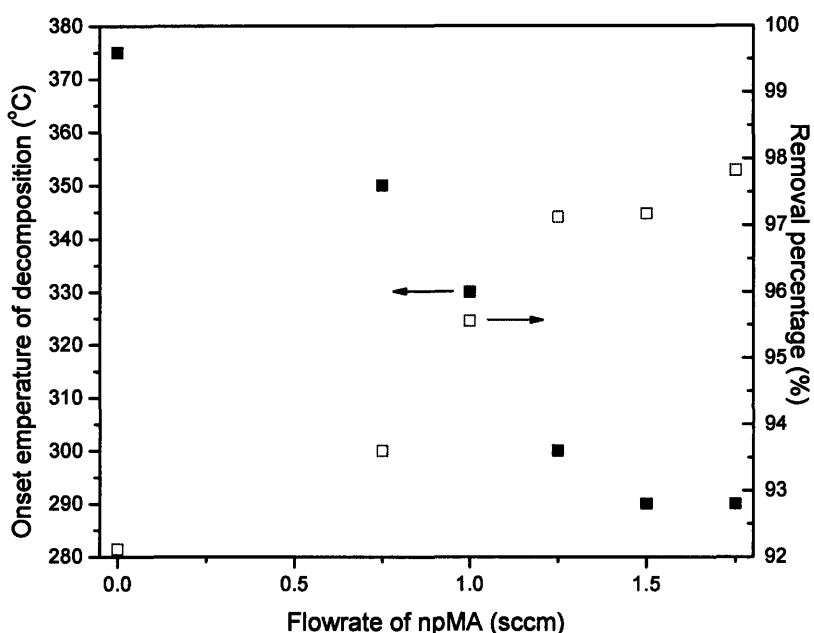


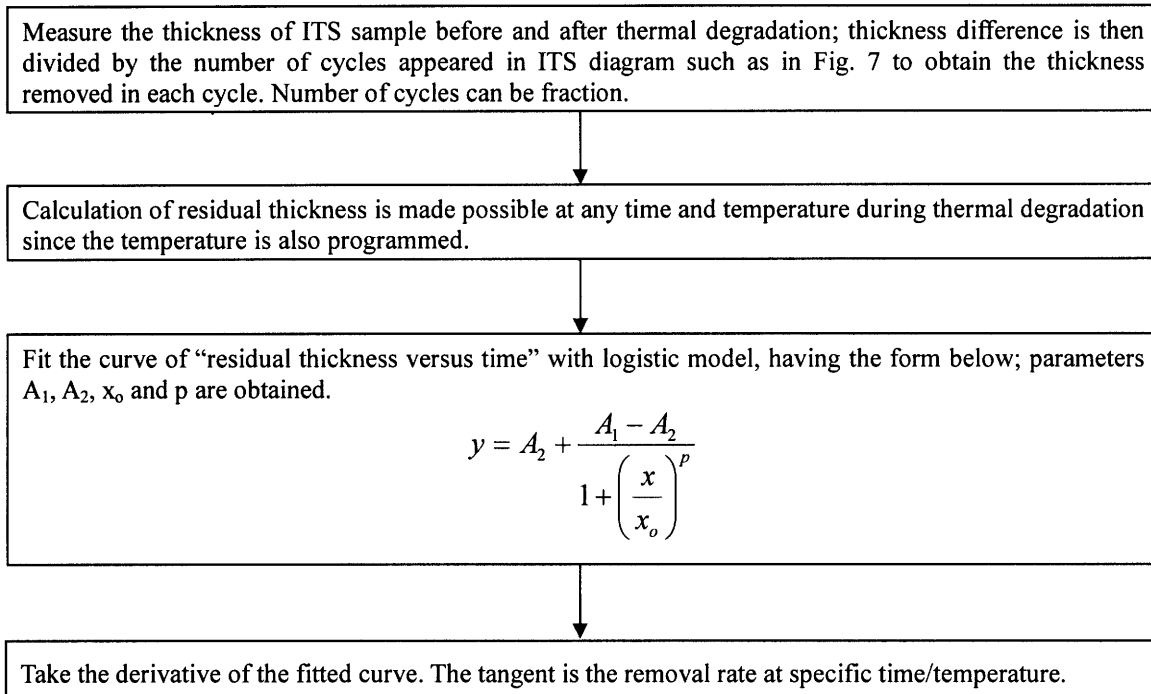
Figure 15: Effect of flowrate of npMA on the onset temperature of thermal degradation and removal percentage

The change in thickness associated with a single cycle of the ITS data was calculated by dividing the thickness difference before and after ITS experiment, as measured by VASE, by the total number of cycles. Data analysis is greatly simplified by extracting thicknesses only at the ITS time points corresponding to the ‘peaks’ and the ‘valleys’ of the cycles. The first derivative of the thickness versus time data at any point is the instantaneous film removal rate. A mathematical description of the entire data set improves the accuracy in determining slope as compared to direct determination at one point in experimental data which contains noise.

The logistic model was found to give an accurate mathematical representation of thickness-time curves. The logistic model was first published by Pierre Verhulst in 1845 and was intended for description of the growth of population²⁶. The rate of population growth increases with the total number of population but is limited by the availability of resources, such as space and food, and eventually the population reaches a maximum the environment can sustain. The logistic model has been applied extensively in biology and economics. The model has the following form:

$$y = A_2 + \frac{A_1 - A_2}{1 + \left(\frac{x}{x_0}\right)^p} \text{ (Eqn. 2)}$$

There are four parameters in the model. A_1 and A_2 are the initial and final value of the process, respectively. P indicates the steepness of growth of population and x_0 is the center point of the time span. In the thermal decomposition process of a P(npMA-co-EGDA) thin film, y is the instantaneous thickness of the film, x is the time of ITS heating, A_1 and A_2 are the initial and final thicknesses, respectively, and x_0 is the time where half of the total removal of the films has occurred. The thermally-induced removal of polymer thin films is the reverse process of population proliferation and is controlled by the chemical reaction (session of covalent bonds) as well as mass transfer process (diffusion and convection). At the initial stage, the removal rate is slow due to the low reaction and mass transfer rates, in spite of the high numbers of potential degradable species. As the temperature increases, chemical bonds gain sufficient energy and bond scission occurs gradually rapidly, resulting in increase of removal rate. However, because the total number of degradable species is fixed, the removal rate starts decreasing despite that the chemical reaction as well as the mass transfer are now sufficiently rapid. Thus the whole process of removal of polymer thin films can be modeled by logistic model. Scheme 1 is a summary of fitting the thickness-time curve with logistic model.



Scheme 1: Flowchart of fitting of "residual thickness versus time" curve

Figure 16 illustrates the variation of thickness versus time of P(npMA-co-EGDA) with $F_{npMA}=1.0$ sccm and the application of logistic model. The R^2 parameter of 0.99876 confirms that the validity of logistic model in describing the change of thickness as time elapsed. The parameters for the five copolymers are listed in table 8, and the initial and final thickness of polymer thin films determined by VASE are attached for comparison. It is noticeable that for $F_{npMA}=0.75$ and 1.0 sccm, A_1 deviate from real thickness more than A_2 ; on the other hand, the value of A_2 is less satisfactory than A_1 for the case of $F_{npMA}=1.25$, 1.5 and 1.75 sccm. Source of the discrepancy may be attributed to the tendency of formation of free radical during thermal decomposition, which is difficult for P(npMA-co-EGDA) copolymers containing low amount of npMA due to the large number of EGDA moieties on the polymer backbone. Monomer-unzipping of P(EGDA) results in formation of less stable secondary free radical which is less likely to evolve at the initial stage when the temperature is not sufficiently high. Therefore the logistic model fails to give a good description for the initial stage of thermal decomposition of P(npMA-co-EGDA) system with lower content of npMA. For the copolymer systems with higher content of npMA, the thermal decomposition takes

place mainly at lower temperature. The thickness remains essentially unchanged even the sample is heated over extended periods and therefore is less well described well by logistic model.

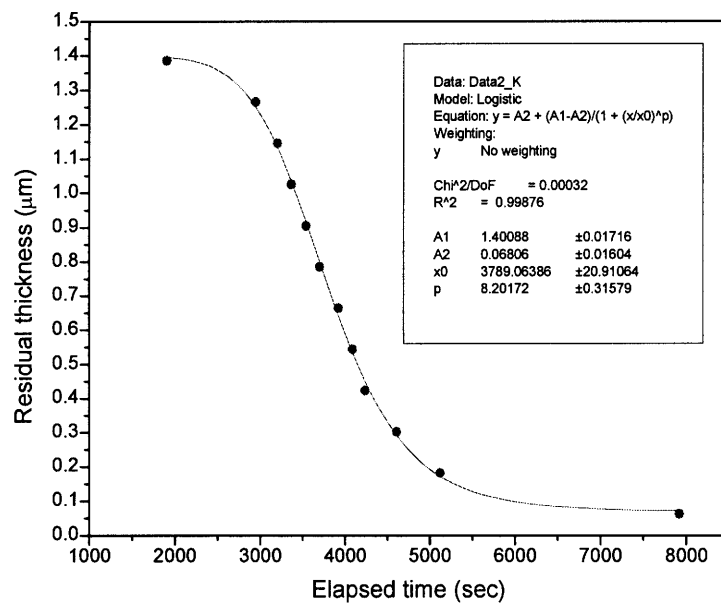


Figure 16: variation of thickness versus time of thermal decomposition of P(npMA-co-EGDA), $F_{npMA} = 1.0\text{sccm}$

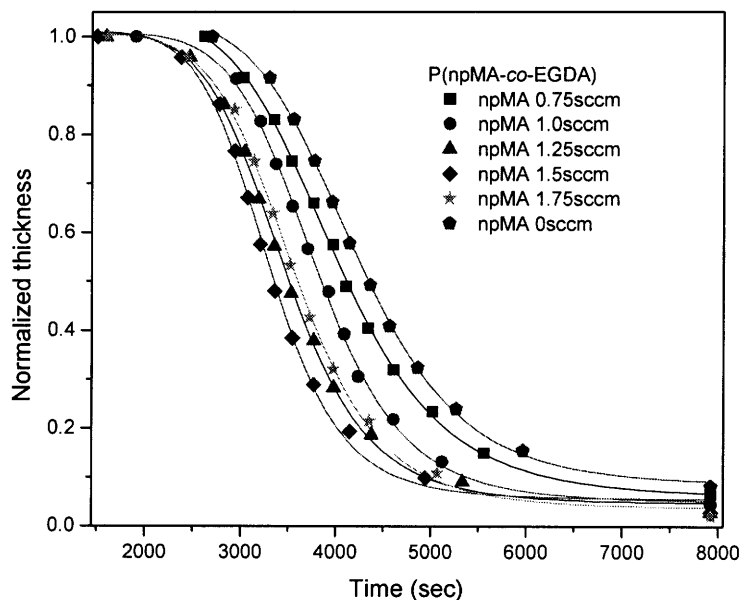


Figure 17: Plot of normalized thickness versus time in ITS for P(npMA-co-EGDA) copolymers

Figure 17 shows the plot of normalized thickness of polymer thin films versus time, which facilitate

visualization of the change in decomposition rates described above. Table 9 and 10 list the fitting parameters of non-normalized and normalized thickness versus time curve, respectively. The parameter A_2 and x_0 show systematic trend of decreasing, which is consistent with the experimental results that as the F_{npMA} increases, both the removal percentage and the removal rate increases.

Table 9: Fitting parameters of removal rate time (without thickness normalization)

F_{npMA} (sccm)	0.75	1.0	1.25	1.5	1.75
A_1	1.442±0.019	1.401±0.017	1.298±0.016	1.284±0.021	1.349±0.015
A_2	0.081±0.013	0.068±0.016	0.059±0.015	0.069±0.019	0.048±0.015
x_0	3988±21	3789±21	3450±21	3295±24	3556±20
P	6.972±0.251	8.202±0.316	7.846±0.336	8.365±0.492	7.825±0.318
Initial thickness *	1.3765±0.0185	1.386	1.279±0.004	1.268±0.001	1.337
Final thickness *	0.0881±0.0032	0.0615±0.0037	0.0368±0.0008	0.0359±0.0001	0.0292±0.0007

*: measured by ellipsometry, μm in unit

Table 10: Fitting parameters of removal rate time (with thickness normalization)

F_{npMA} (sccm)	0.75	1.0	1.25	1.5	1.75
A_1	1.048±0.012	1.009±0.011	1.012±0.011	1.010±0.015	1.007±0.010
A_2	0.059±0.010	0.050±0.012	0.047±0.011	0.055±0.015	0.037±0.011
x_0	3988±19	3790±20	3453±20	3297±23	3558±20
P	6.964±0.243	8.240±0.307	7.900±0.331	8.705±0.484	7.866±0.312

The instantaneous removal rate was determined by differentiating the mathematical expression of the model with respect to time and inserting the parameters and the time of interest:

$$\frac{\partial y}{\partial x} = (A_2 - A_1) \frac{\frac{p}{x} \left(\frac{x}{x_0}\right)^{p-1}}{1 + \left(\frac{x}{x_0}\right)^p} \quad \text{----- (Eqn. 3)}$$

Since each time also corresponds to a specific temperature, the apparent activation energy and pre-

exponential factor in Arrhenius expression for thermal decomposition can therefore be extracted. Table 11 and 12 list the kinetic data of thermal decomposition of the five P(npMA-co-EGDA) copolymers and the Arrhenius plot is shown in figure 18. The copolymers of P(npMA-co-EGDA) $F_{npMA}=0.75$ sccm and 1.0 sccm were treated separately due to their higher onset temperatures of decomposition.

Table 11: Removal rate ($\mu\text{m}/\text{min}$), pre-exponential factor and activation energy at selected temperatures

F_{npMA}	1.25sccm	1.5sccm	1.75sccm
325°C	0.0024	0.0023	0.002
350°C	0.0077	0.0088	0.0066
375°C	0.0262	0.0328	0.0231
Pre-exponential factor	6.85×10^{10}	4.36×10^{11}	5.03×10^{11}
Activation energy (kJ/mol)	154.7	164.2	162.3

Table 12: Removal rate ($\mu\text{m}/\text{min}$), pre-exponential factor and activation energy at selected temperatures

Temperature\Flowrate	0.75sccm	Temperature\Flowrate	1.0sccm
375°C	0.0134	350°C	0.0059
380°C	0.0173	360°C	0.0101
385°C	0.0216	370°C	0.0169
390°C	0.0273	380°C	0.0285
395°C	0.0329	390°C	0.0418
Pre-exponential factor	1.72×10^{11}	Pre-exponential factor	1.07×10^{12}
Activation energy (kJ/mol)	162.6	Activation energy (kJ/mol)	169.9

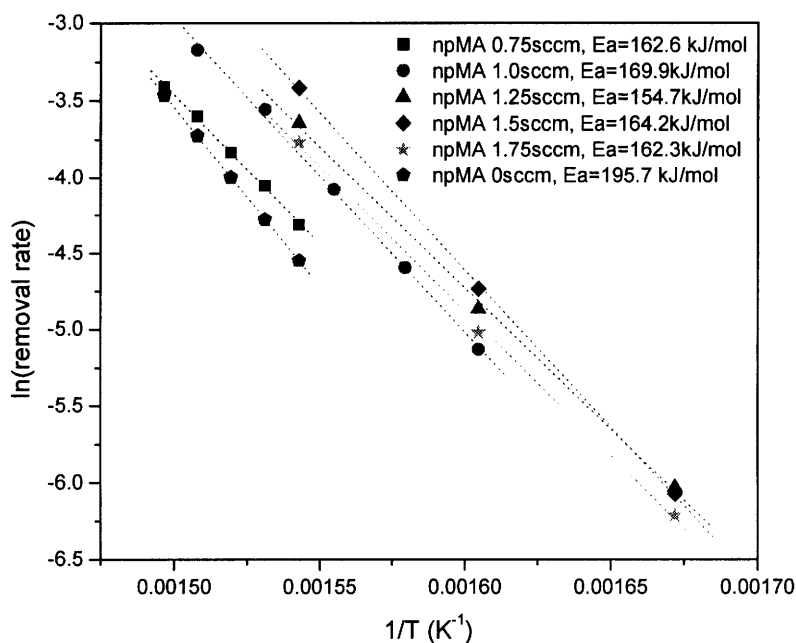


Figure 18: Arrhenius plot of removal rate versus temperature

For all of the P(npMA-co-EGDA) copolymers, similar values were obtained for the apparent activation energies 162.7 ± 8 kJ/mol. This similarity suggests that the same rate-determining reaction occurs at each composition and there is no composition-dependent side reaction in addition to thermal decomposition. The activation energies for different composition of copolymers are expected to be approximately the same if the rate-determining steps are the same and there is no composition-dependent side reaction in addition to thermal decomposition. The activation energies are 162.7 ± 8 kJ/mol and the standard deviation is 5.43 kJ/mol, which is less than 3.5% of the activation energy obtained. Furthermore, it matches the reported value of 37 kcal/mol¹ (which is equivalent to 155.4 kJ/mol) for thermal decomposition of poly(methyl acrylate) fairly well. This indicates the rate-determining step is the decomposition of EGDA moieties which have higher thermal stability compared to npMA; the general activation energy of polymethacrylates was reported to be within the range of 25 kcal/mol¹ (104.6 kJ/mol). Figure 19 shows the variations in activation energy and the pre-exponential factor with flowrate of npMA. The pre-exponential factors are more scattered in the range of 10^{10} to 10^{12} and the largest value is 15 times the lowest value, but still they are within the reasonable range³.

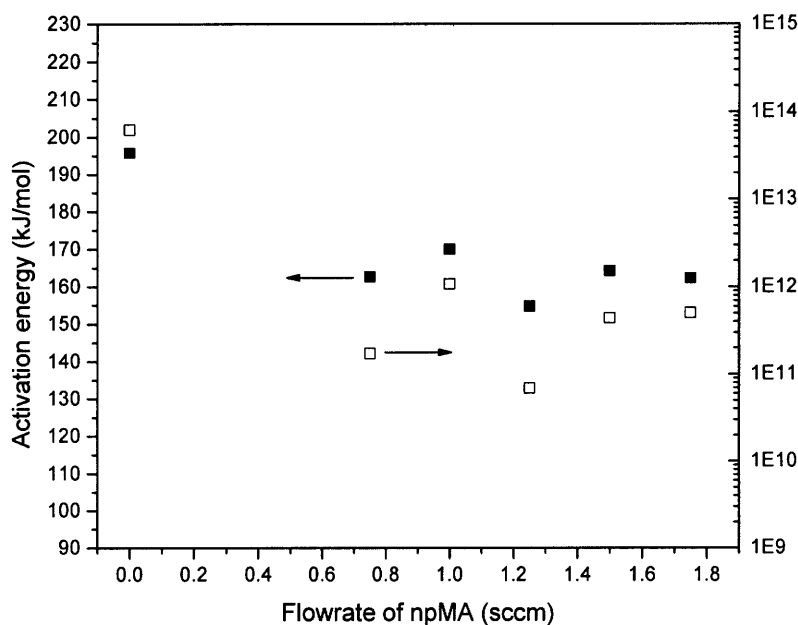


Figure 19: Activation energy of removal of P(npMA-*co*-EGDA) versus flowrate of npMA

It is interesting that the activation energy of P(EGDA) homopolymer is higher than the copolymers by more than 30 kJ/mol since the rate determining step is expected to be the same. This might be attributed to the higher crosslinking density of the homopolymer. When a bond on the backbone dissociates and form two radicals, the surrounding prevents the diffusion of these radicals due to high crosslinking density and the probability for the two radical to recombine will be much higher than it is if the radicals are less confined to move around. This is the so-called cage effect.¹ Under the influence of the cage effect, more thermal energy is require to effectively separate the two radicals and therefore the activation energy is higher.

Flash pyrolysis gas chromatography mass spectroscopy

Application of sacrificial materials in IC integration process requires that the thermal degradation products diffuse through common dielectrics such as silicon oxides or silicon nitrides, therefore it is essential to understand the composition of degradation products mixture to optimize the diffusion rate and percentage by tuning the pore size and/or porosity of overlayer. In this thesis, flash pyrolysis experiments followed by gas chromatography coupled mass spectroscopy (FP-GCMS) were performed to elucidate the composition of thermally degraded products of P(npMA), P(EGDA) and P(npMA-*co*-EGDA). P(npMA-*co*-EGDA) with $F_{npMA} = 1.0$ sccm was used as a representative sample for copolymers.

Figure 20 to 22 serve as the standards for identifying npMA and EGDA monomers in GCMS results of thermal degradation products of iCVD films. Figure 20 shows the gas chromatograms of npMA and EGDA monomers; figs. 21 and 22 are the mass spectra (MS) for the npMA and EGDA monomers, respectively. Four groups of peaks were observed in figure 21 with m/z of 41, 57, 69 and 101 as the major peak in each group, representing propenyl, *t*-butyl, 2-methylethenylcarbonyl and methacryloyl methylene group, respectively. Only one intense peak with m/z of 55 was present in figure 22 which represents ethenylcarbonyl group. Figure 20 to 22 serve as the standards for identifying npMA and EGDA monomers in GCMS results of thermal degradation products of P(npMA), P(EGDA) and P(npMA-*co*-EGDA) since the conditions of column separation were kept the same.

The GC chromatogram of P(npMA) degradation products is shown in figure 23. The largest peak is observed 10.617 min. and has the same retention time as observed in GC spectrum of npMA monomer in figure 21. The mass spectra for both peaks in Figure 21 and 24 are also the same. Therefore, npMA monomer is a clearly identified as the primary degradation product of iCVD P(npMA), supporting the the hypothesis of the monomer-unzipping mechanism.

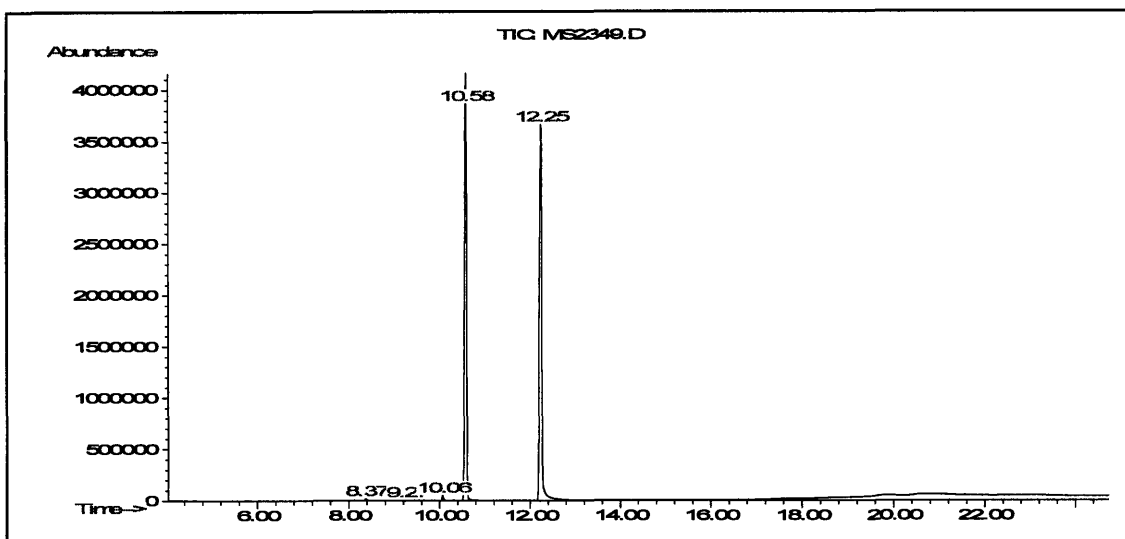


Figure 20: GC chromatogram of npMA and EGDA monomers

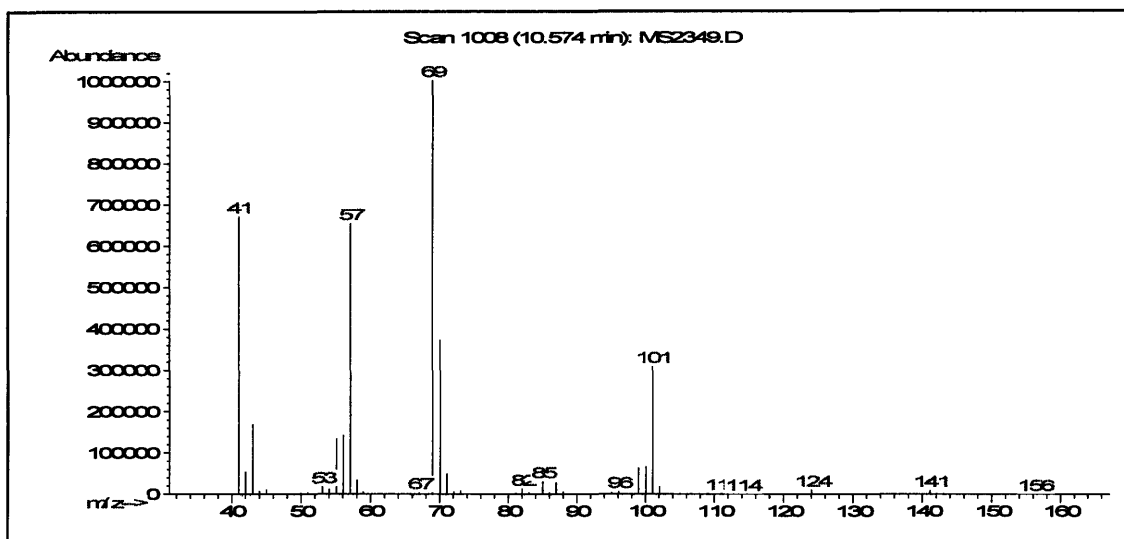


Figure 21: MS spectra of npMA (m.w.: 156 Da)

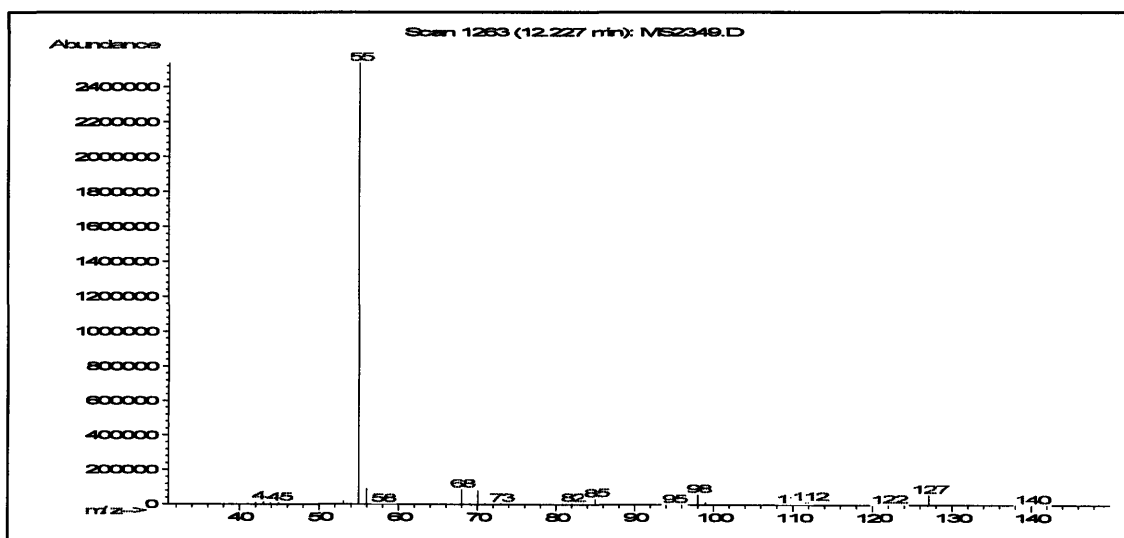


Figure 22: MS spectra of npMA (m.w.: 170 Da)

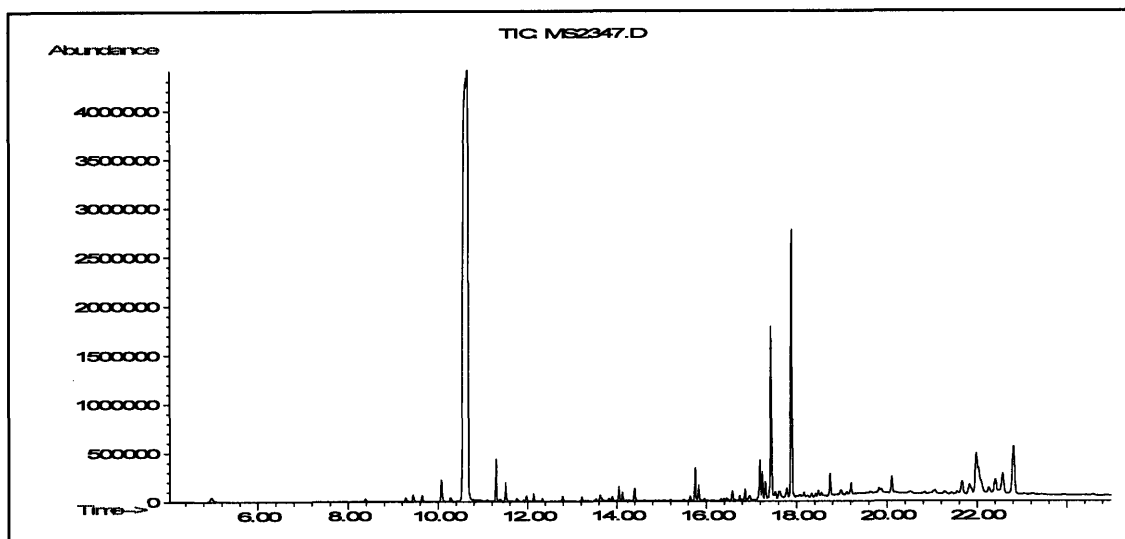


Figure 23: GC chromatogram of decomposition product of P(npMA)

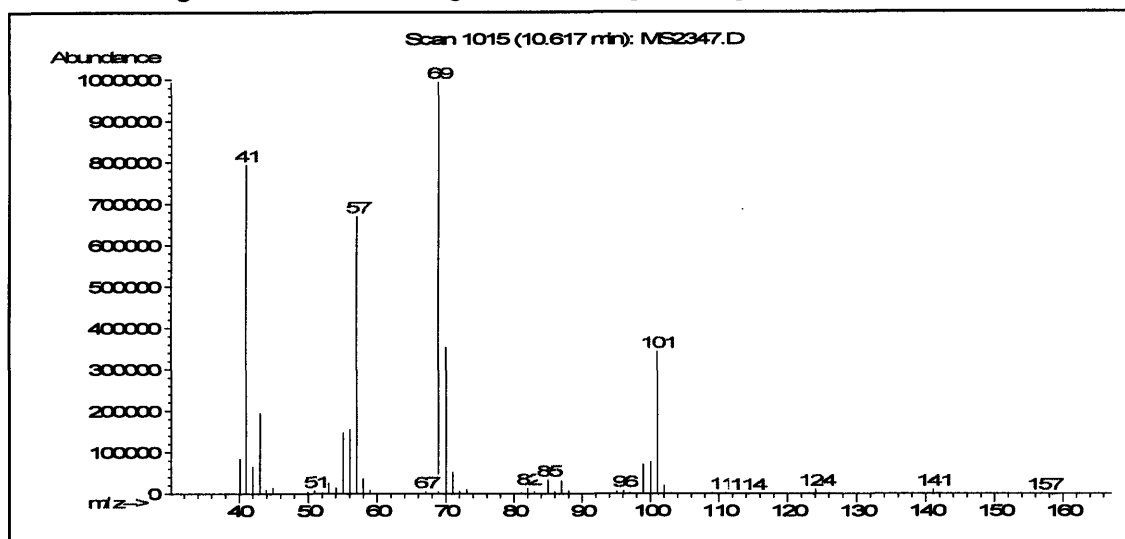


Figure 24: MS spectra of the peak at 10.617min

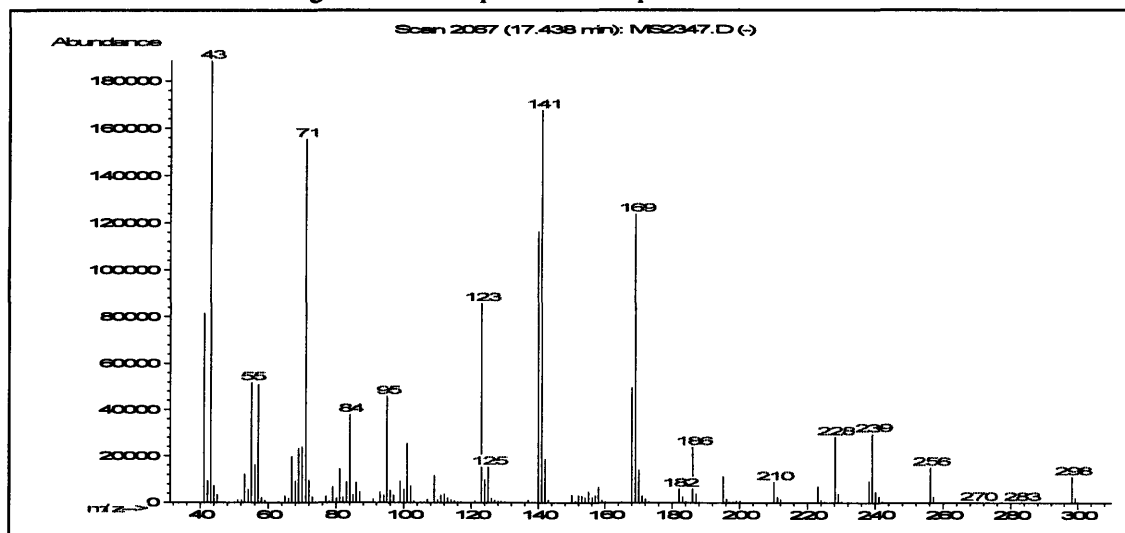


Figure 25: MS spectra of the peak at 17.438min

Monomeric decomposition products are desirable since their dimensions are small, facilitating rapid and complete diffusion through any overlayer required for air gap fabrication. Two additional peaks of significant intensity were observed in figure 23 at 17.438 min. and 17.892 min. The MS spectrum of the peak at 17.438 min. is shown in figure 25. It is speculated that these two peaks are associated with the npMA dimers, since many of the peaks are closely associated with the potential fragments of dimerized npMA. The peak with m/z equal to 298 in Figure 25 and 255 in the mass spectrum of the peak at 17.892 min. (not shown) represents [M-14] and [M-57] where M is 312, the molecular weight for npMA dimer. [M-14] and [M-57] species stand for dimers in which a methylene and a tert-butyl group has been lost due to electron impact, respectively. The different elution time might be attributed to the different structures of these dimers due to extensive rearrangements during pyrolysis so that the polarities are slightly varied. The presence of npMA dimers might be related to the relatively small size and hence the high vapor pressure which results in their escaping from the heated point in the furnace before complete monomer unzipping occurred. It is expected that the percentage of oligomeric thermal decomposition products will decrease in real process where the temperature ramping will be milder in order to prevent the overlayers from cracking or delaminating due to the pressure buildup of volatile decomposition products, since the oligomers will have sufficient time to dissociate into monomers.

Peaks in mass spectra due to incorporation of initiator fragments, tert-butoxy groups ($m/z = 73$), in polymer backbones were also considered; however, the small percentage of number of initiator fragments (1 or 2 tert-butoxy moieties per chain versus several hundreds of repeating unit) as well as the difficulty of formation of t-butoxy cation (in order to be detected) due to localization of positive charge on electronegative oxygen atom make it less likely to determine the presence of initiator fragments as endgroups using FP-GCMS in a positive and confirmative way.

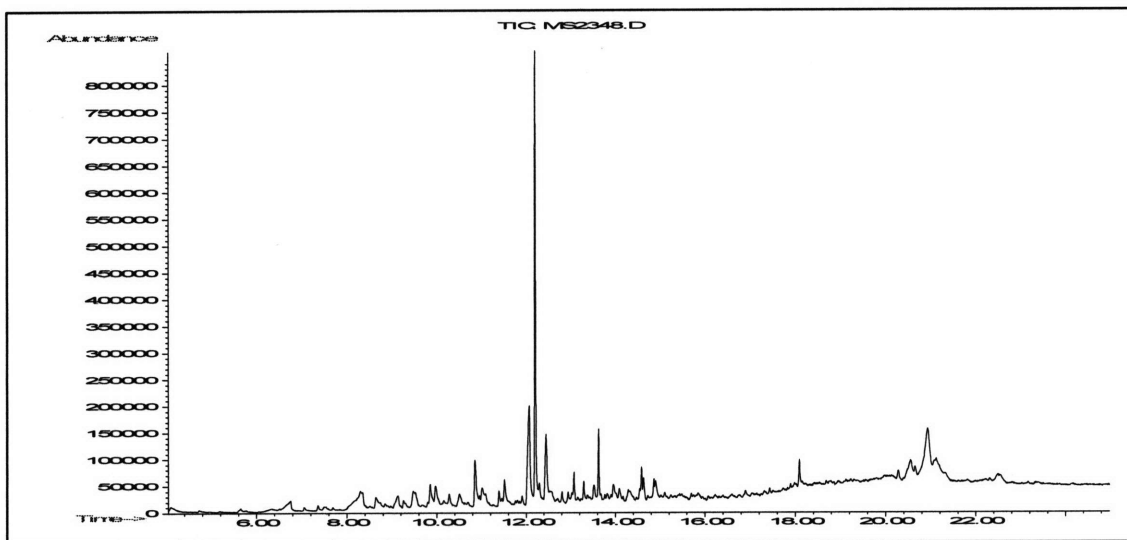


Figure 26: GC chromatogram of decomposition product of P(EGDA)

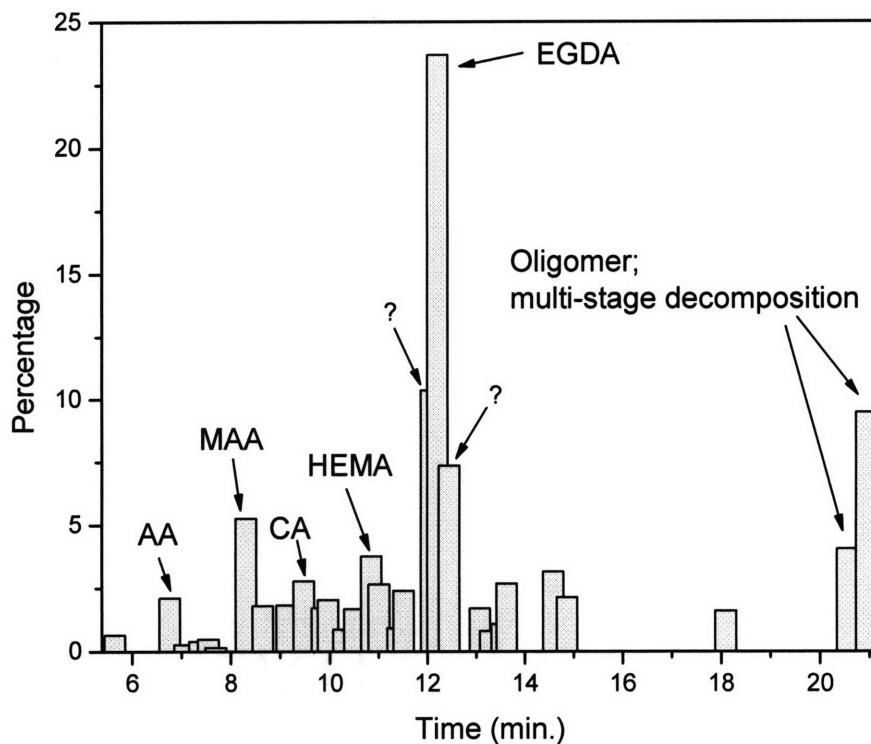


Figure 27: Percentage of peak area of P(EGDA) decomposition products in GCMS analysis

Figure 26 shows the GC chromatogram of P(EGDA) degradation product. Numerous small peaks were observed in addition to the EGDA peak at 12.204 min. Polyacrylates have been known to degrade via several mechanisms³, such as monomer unzipping, random scission along polymer backbone, fragmentation of groups either on polymer backbone or side groups, etc., hence the

multiple peaks. Figure 27 is the distribution plot of percentage of peak area versus time at which individual peak appears. Species that have been identified are labeled in the figure such as acrylic acid (AA), methacrylic acid (MAA), crotonic acid (CA), 2-hydroxyethyl methacrylate (HEMA) and EGDA monomers. Many of the peaks however were beyond recognition, implying the complexity of rearrangement /recombination reactions during degradation. The peaks at 12.073 and 12.445 min. are two of these unidentified peaks and, because of their comparatively large peak area, it is of practical importance to understand what they represent, at least qualitatively. It is believed they are the derivatives of methacrylates and acrylates, respectively; the former has the characteristic peak of m/z of 70 (usually varies in the range of 69~71) and the latter has characteristic peak of m/z of 56 (varies in the range of 55~57). Peaks with m/z value of 55 and 69 have been reported as the base peak of acrylate and methacrylate monomers²⁷ in mass spectroscopy, and they represent the ethenylcarbonyl cation and 2-methylethenylcarbonyl cation, respectively. Both are stabilized due to delocalization of positive charge and are thus easily generated. Higher oligomers are also present in the degradation products since the MS spectra of those peaks with retention time higher than 20 minutes in GC chromatogram showed there are peaks of large area at m/z of 297 and 300.

Carbon dioxide is also one of the decomposition products during P(EGDA) degradation based on the results of thermal degradation of poly(methyl acrylate) (PMA) where carbon dioxide were observed in large quantity and a mechanism has been proposed by Madorsky¹⁻² in which intramolecular abstraction of hydrogen atom occurs on polymer backbone and results in formation of ester radicals. The ester radicals then form carbon dioxide and leave the radical on the polymer backbone. In this study, 2-hydroxyethyl methacrylate (HEMA) was observed at 10.851 min. in GC chromatogram, which is a product following the generation of carbon dioxide and intramolecular proton shift. However, carbon dioxide could not be observed by GCMS since its retention time is so short compared to the solvent methylene chloride in the GC column and the platinum filament in MS has to be turned off before the arrival of solvent molecules to avoid saturation of signal and

possible damage to the filament. It is difficult to exclude the possibility of carbon monoxide and water but there was no evidence to sustain their presence in the pyrolysis products mixture.

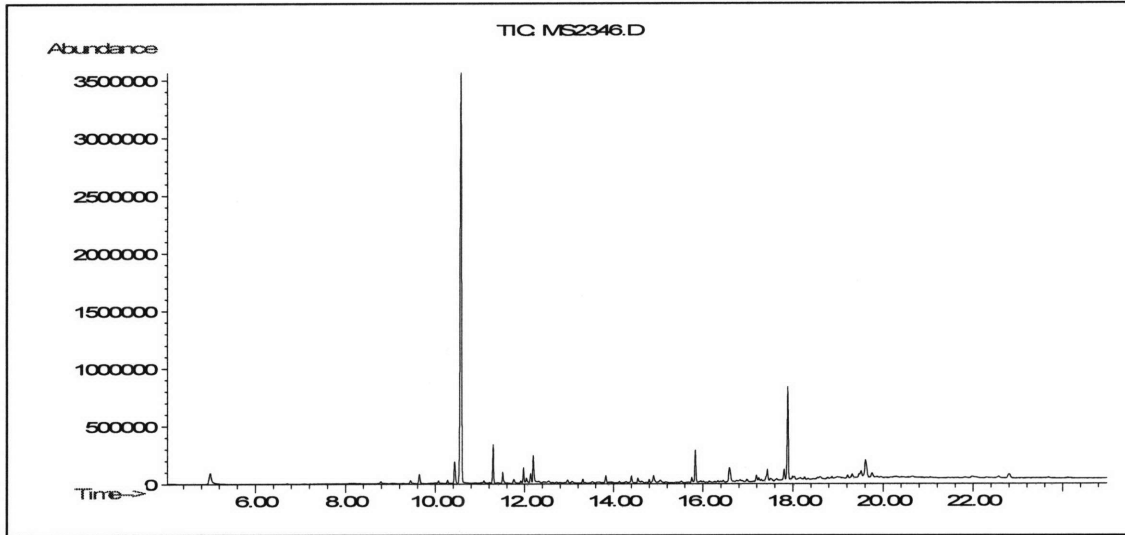


Figure 28: GC chromatogram of decomposition product of P(npMA-co-EGDA)

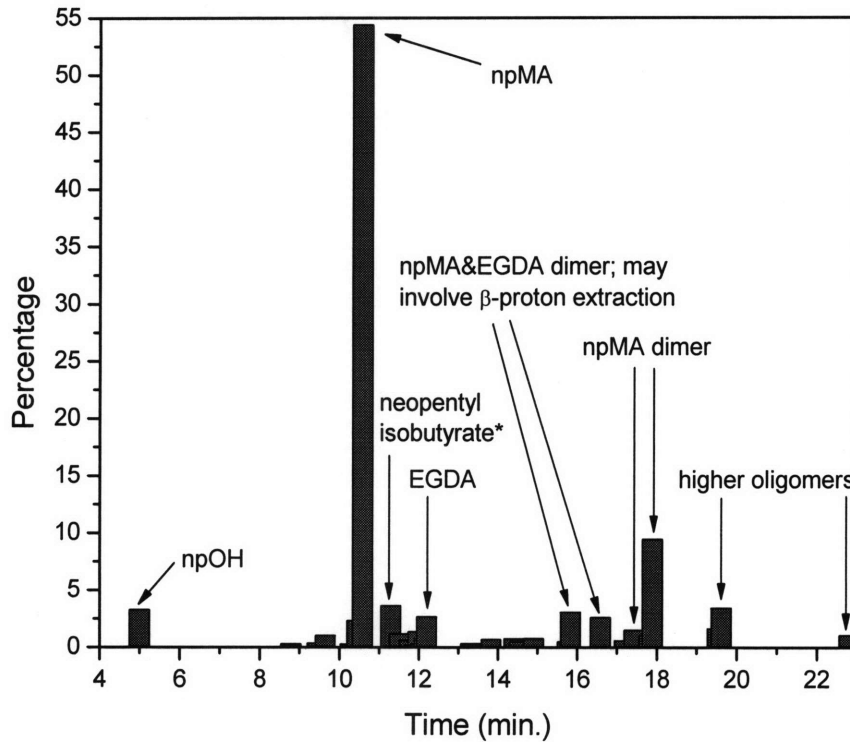


Figure 29: Percentage of peak area of P(npMA-co-EGDA) decomposition products in GCMS analysis

Figure 28 is GC chromatogram of degradation products of iCVD P(npMA-co-EGDA) deposited with $F_{npMA}=1.0$ sccm, and figure 29 shows the distribution plot. npMA and EGDA monomers were

observed as expected. Most of the npMA moieties escaped in the form of monomer. The percentage of EGDA monomers evolved was much lower (2.7%) than that in the case of pyrolysis of P(EGDA) homopolymer (23.7%) which might be related to the comparatively less crosslinked structure in the copolymer and thus the higher probability of reactions between side groups and fragmentation. There were other decomposition products such as neopentyl alcohol (product of alpha-cleavage of groups next to carbonyl, which also appeared in insignificant amount (0.4%) in pyrolysis product of P(npMA)), neopentyl isobutyrate (product of random scission along the polymer backbones of npMA segments), npMA-EGDA dimers, npMA dimers, and higher oligomers. And finally, carbon dioxide was expected to be among the pyrolysis product. Table 13 summarizes the volatile products detected during FP-GCMS analysis.

Figure 30, 31 and 32 demonstrate the TGA chromatograms of P(EGMA), P(npMA-co-EGDA) and P(npMA), respectively. P(npMA) started to decompose around 175 °C, which is quite low for polymethacrylates. One of the explanations is that some volatile monomers/oligomers might have been trapped in polymer matrices and evolved quickly under elevated temperature. P(npMA)

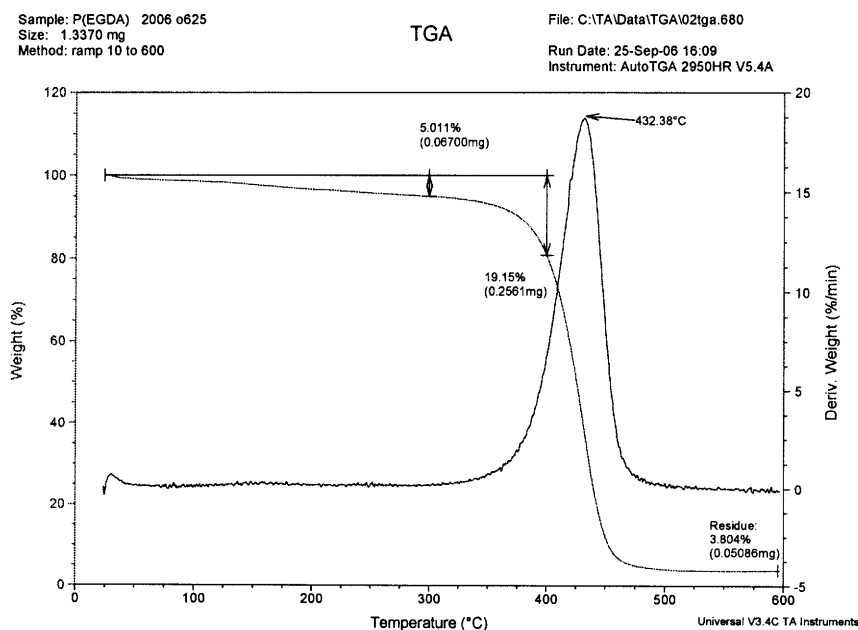


Figure 30: TGA thermogram of P(EGDA)

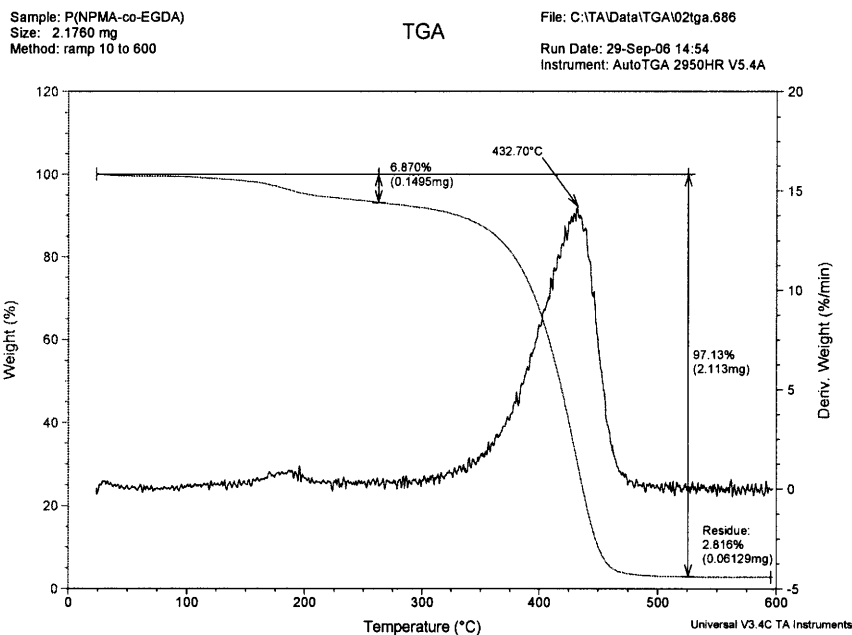


Figure 31: TGA thermogram of P(npMA-co-EGDA)

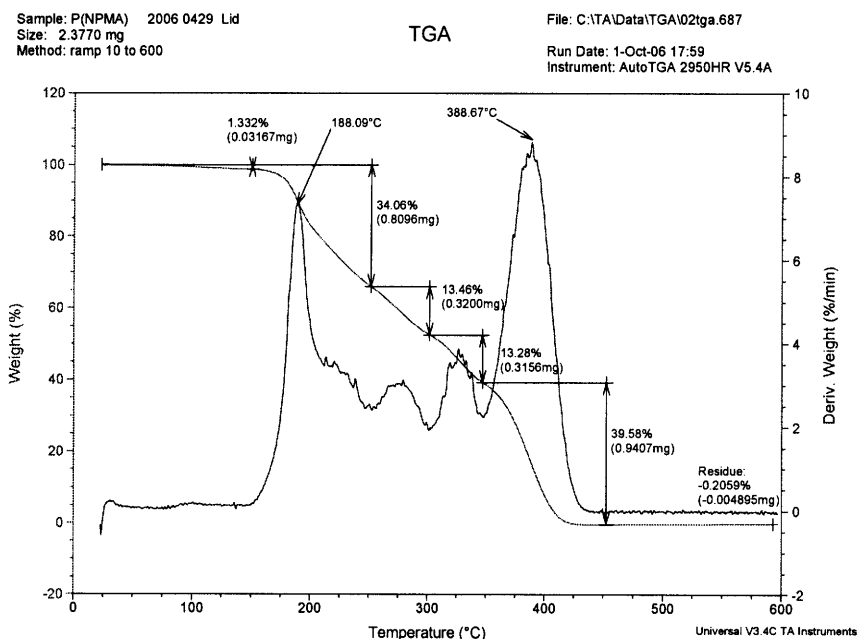


Figure 32: TGA thermogram of P(npMA)

decomposed completely around 425 °C. On the other hand, P(EGDA) was much more thermally stable than P(npMA); major decomposition did not occur until 350 °C and the residue at 600 °C was 3.8%. When npMA and EGDA monomers were copolymerized, the thermal stability improved dramatically; the onset temperature of decomposition became 325 °C and the residue at 600 °C was

2.8%. The TGA experiments conducted on bulk samples also confirmed the feasibility of the idea of using P(npMA-*co*-EGDA) crosslinked copolymer as potential sacrificial materials in thermal aspect.

The potential drawbacks of FP-GCMS include (1) the temperature and the duration of pyrolysis has very strong effects on the species and the amounts of volatilization of samples. Linear poly(methyl acrylate) has been reported to volatilized to 96.8% at 399 °C for thirty minutes². In the present study, P(EGDA) and P(npMA-*co*-EGDA) samples are crosslinked and the pyrolysis was conducted at 400°C for five minutes only. Therefore lower volatilization percentage is expected. (2) Oligomers of large sizes may not able be able to travel far enough to the end of GC column in the limited time set by the GC due to their low tendency of volatilization, thus the GC chromatogram might not show the entire spectrum of thermal degradation products. (3) The area percentage in GC chromatogram only reflects the relative amounts of species but not the weight percent since the responding coefficients of different species may vary as much as 5. In the ITS tests of homo- and copolymer samples deposited on silicon wafer and in practice however, heating duration (30~60 minutes) are much longer than the flash pyrolysis time, and volatilization percentage of polymer samples and transport of degradation products is expected to be better.

Table 13: Results of flash pyrolysis of homo- and copolymers of P(npMA-co-EGDA)

Polymer	Degradation mechanism	Main volatile product; percentage in parenthesis
P(npMA)	<p>Monomer-unzipping: Depolymerization along polymer backbone</p>	<ul style="list-style-type: none"> • Neopentyl alcohol: 0.4% • Isopropyl methacrylate: 0.2% • Neopentyl acrylate: 0.2% • npMA monomer: 59.4% • npMA dimer: 16.5% • Higher oligomer: 7.5% • Unidentified species: 15.8%
P(EGDA)	<p>Fragmentation: Cleavage of chemical bonds occur on the polymer backbones and side groups as well</p>	<ul style="list-style-type: none"> • Acrylic acid: 2.1% • 2-methylpropanoic acid: 0.5% • Methacrylic acid: 5.3% • 2-methylbutanoic acid: 1.8% • Crotonic acid: 2.8% • 4-hydroxy-2-butenoic acid: 0.9% • 2-hydroxyethyl methacrylate: 3.8% • 2,2-dimethylpropyl propanoate: 2.7% • Unknown species 1: 10.4% • EGDA monomer: 23.7% • Unknown species 2: 7.4% • Total unidentified species: 58%
<p>P(npMA-co-EGDA), $F_{npMA} = 1.0\text{scm}$</p>	<p>Monomer-unzipping and fragmentation: Both mechanism occurred during thermal degradation</p>	<ul style="list-style-type: none"> • Neopentyl alcohol: 3.3% • npMA monomer: 54.5% • Neopentyl isobutyrate: 3.6% • EGDA: 2.7% • npMA dimer: 5.6% • npMA-EGDA dimer: 10.9% • Higher oligomers: 6.1% • Unidentified species: 13.3%

Residue on substrate after thermal degradation: FTIR and XPS analysis

The residue on the substrates affects the electrical properties of final circuits and therefore it is desirable to understand the species that are present after thermal decomposition. Figure 33(A) shows the FTIR spectrum of P(npMA-co-EGDA) with $F_{npMA} = 1.0$ sccm before and after ITS experiment. It is clear that the ratio of peak intensity of carbonyl stretching (1735 cm^{-1}) to C-H stretching ($2800\sim 3000\text{ cm}^{-1}$) changed substantially after thermal annealing. Broadening of the carbonyl peak was observed after thermal annealing and there were peak shoulders at³⁰ 1770 cm^{-1} and 1810 cm^{-1} . These two peaks indicated the presence of six-membered cyclic anhydrides, which is the product of proton abstraction by ester oxygen atoms on the side group of copolymer followed by dehydration. The peaks at 1600 cm^{-1} (carbon-carbon double bond stretching mode in aromatic systems) and 3050 cm^{-1} (C-H stretching in aromatic systems) imply the formation of aromatic rings during thermal annealing. The cyclic anhydrides and aromatics are more thermally stable compared to linear aliphatic structures, and FTIR confirmed that these species were indeed present in residues. In figure 33(A) the FTIR spectrum of P(EGDA) homopolymer after ITS experiment was added for comparison. The spectrum of P(npMA-co-EGDA) with $F_{npMA} = 1.0$ sccm and P(EGDA) after annealing are very similar, which implies that EGDA is the primary contributor to the residue and the presence of npMA in the copolymer does not contribute significantly to the chemical nature of residue.

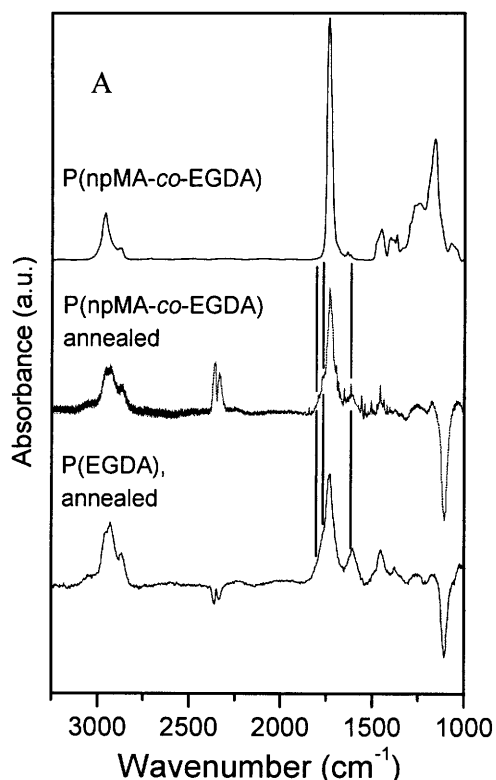


Figure 33 (A): FTIR results of residue on silicon wafer after heating at 400C for 1hr under N_2

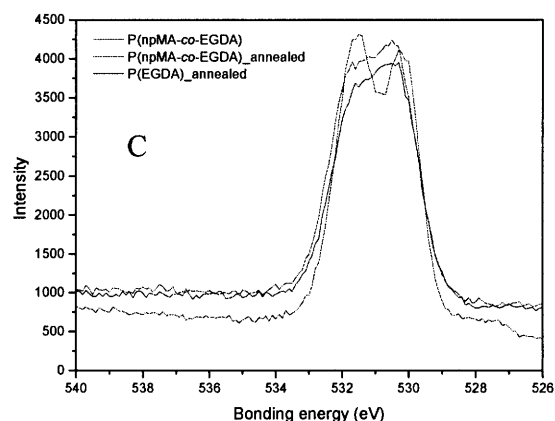
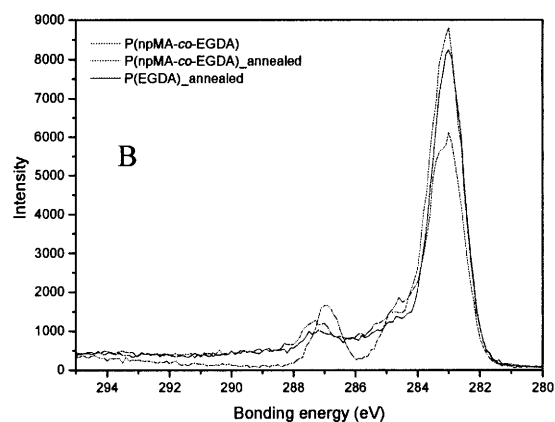


Figure 33(B), (C): FTIR and XPS results of residue on silicon wafer after thermally-treated at 400C for 1hr under N₂

Figure 33(B) and 33(C) show the XPS high resolution scan on carbon and oxygen on P(npMA-co-EGDA) before and after ITS experiments, respectively. The carbon peaks after thermal annealing became broader and less distinguished in the region of 284~286eV. The carbonyl peak broadened and shifted toward the higher energy as well. Figure 34 shows the qualitative curve fitting results for XPS spectrum of P(npMA-co-EGDA) with $F_{npMA} = 1.0$ sccm before and after thermal annealing. The areas of the two peaks in figure 34(A) are approximately the same (532.01eV (carbonyl oxygen): 49%, 530.60eV (ester oxygen): 51%) while it takes at least three peak to fit figure 34(B) well (532.12eV: 22%, 531.51eV: 6%, 530.52eV: 72%), which indicates the chemical structure for a significant proportion of the oxygen atoms became different after thermal annealing. The peak at 531.35eV is believed to be due to the anhydride oxygen atom.

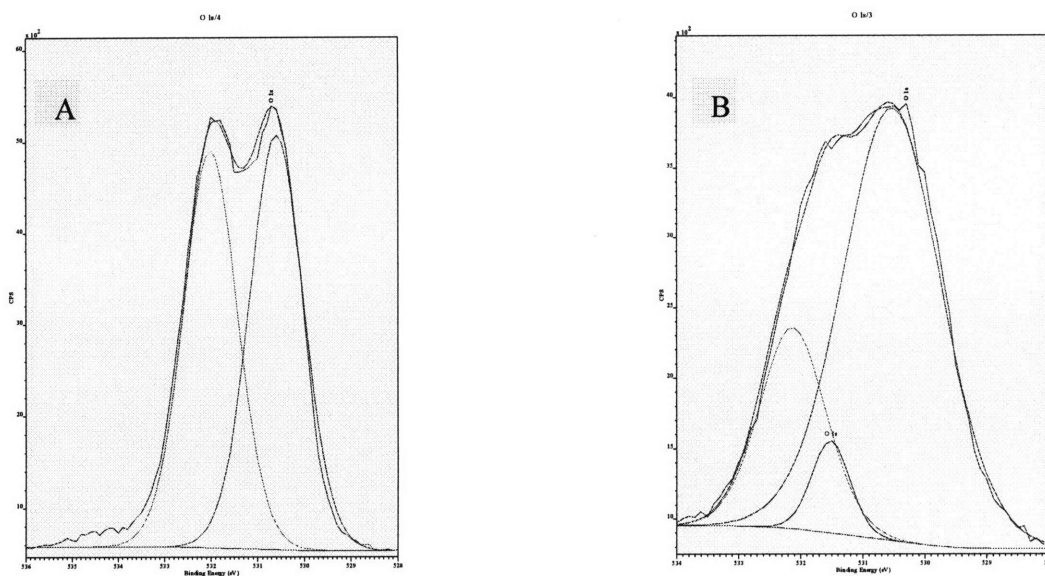


Figure 34: (A) Fitting of P(npMA-co-EGDA) before ITS, (B) Fitting of the same sample after ITS

Nanoindentation: Young's modulus and hardness

During the integration process for IC, the sacrificial material for construction of air-gap structure will be subjected to mechanical stress while undergoing processes such as chemical mechanical polishing⁴⁵ (CMP) and flip-chip bonding⁴⁶. Therefore it is essential to have good mechanical properties in order to retain the integrity of the sacrificial material. Nanoindentation experiments were conducted on the series of P(npMA-*co*-EGDA) copolymers and on the homopolymers of P(npMA) and P(EGDA) to determine the values of the Young's modulus and the hardness.

The modulus and hardness of P(npMA), P(EGDA) and P(npMA-*co*-EGDA) are listed in table 14. The standard deviation for both mechanical properties are small compared to the measured values (<5%), implying the uniformity of the deposition. Figure 35 shows that the moduli of the copolymers gradually decreases as the content of npMA in P(npMA-*co*-EGDA) increases, which is expected since the polymer matrices become less restricted and more mobile to external forces when the crosslinking densities decrease. Figure 35 also shows that the values of hardness show the same trend. For comparison, the modulus and the hardness of PMMA obtained from bulk mechanical test are 3.3 GPa and 0.195 GPa, respectively. The crosslinked copolymers are expected to be superior to linear PMMA in mechanical properties and indeed they are.

The result shows that the modulus for P(npMA) homopolymer is the highest among the seven samples, which is contrary to expectation at the first glance. Neopentyls are bulky side groups and theoretically tend to stay away from one another in a polymer chain, and the anti conformation of neighboring neopentyl groups should give the lowest energy. Therefore, if the conformations of every single neighboring pair, or a large proportion of these pairs, are anti, the entire chain/segment is syndiotactic and the total energy of the chain is at its lowest possible state.

Table 14: Young's moduli and hardnesses of P(npMA-co-EGDA)

F_{npMA} (sccm)	Young's modulus (GPa)	Standard deviation of modulus (GPa)	Hardness (GPa)	Standard deviation of hardness (GPa)
0.75	4.93~5.37	0.122	0.67~0.73	0.019
1.0	4.79~5.28	0.108	0.53~0.57	0.014
1.25	4.38~4.88	0.180	0.48~0.53	0.016
1.5	4.35~4.81	0.186	0.44~0.51	0.019
1.75	3.97~4.60	0.186	0.39~0.47	0.036
P(npMA)	5.46~5.83	0.097	0.62~0.71	0.022
P(EGDA)	4.72~5.08	0.240	0.81~0.87	0.035

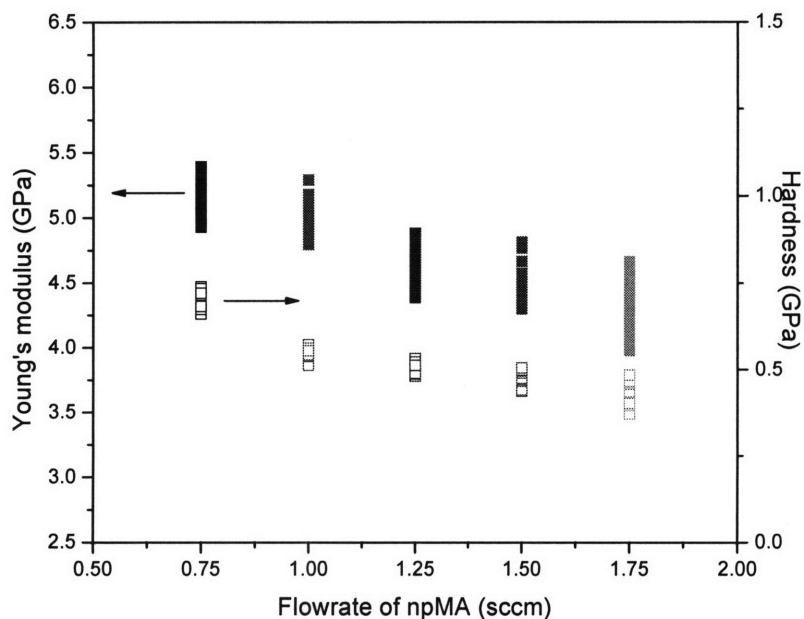


Figure 35: Effect of flowrate of npMA on the Young's modulus and hardness of copolymers

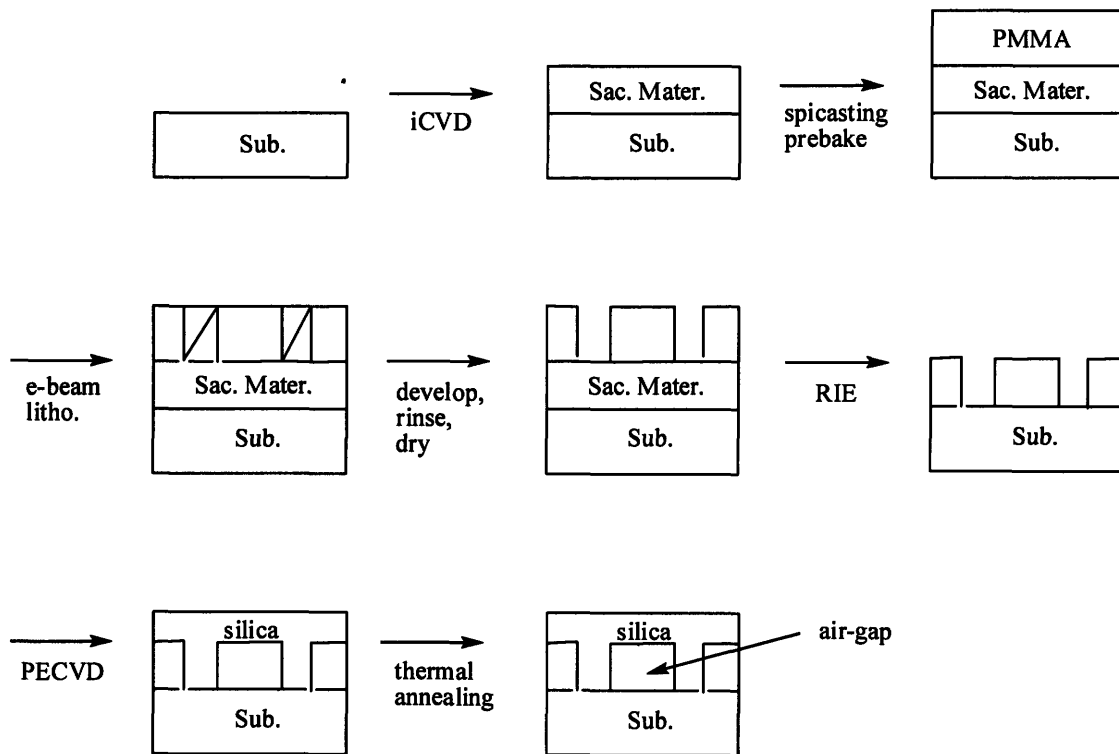
Because of the stereoregularity of the side group arrangement, syndiotactic chains tend to have more compact packing and the chain mobility is lowered appreciably. If this were the case, the mechanical properties would have been expected to improve even though the material is solely composed of linear polymer chains. However in the NMR spectrum of P(npMA) in figure 8, the splitting pattern of methylene proton peak on polymer backbone reveals that the P(npMA)

synthesized by iCVD cannot be stereoregular over the entire chain because syndiotactic polymethacrylate show single peak in this region²⁵. Nonetheless the *rrr* tetrad peak at 1.87 ppm indicates the anti conformation is adopted by a large number of neighboring neopentyl groups and therefore ordered arrangement of side groups on a smaller scale (local region) is still likely which results in limitation of the chain mobility and enhances the mechanical properties. In spite of the superior mechanical properties, P(npMA) is not considered as a potential candidate for air-gap sacrificial materials due to the low thermal stability as shown in Table 2-2.

The moduli and the hardnesses of homopolymers in table 14 are both higher than the copolymers and thus the mixing rule does not apply in the study. Additional interaction between two monomeric units is likely and the copolymer is more than a simple two-component mixture. Addition of npMA moieties to P(EGDA) increases the chain length between crosslinking points (M_c) along the polymer backbone and free volume between chains, facilitating the thermal motion of copolymers. Addition of EGDA to P(npMA) is believed to disrupt the local arrangement of neopentyl side groups and the inherently long distance of EGDA (dimension of EGDA: 11.45 Å * 5.15 Å * 2.78 Å, simulated by Gaussian software) between the two polymerizable group is also expected to increase the interchain distance. To summarize, P(npMA-*co*-EGDA) copolymers have Young's modulus between 3.97 to 5.37 GPa and hardness between 390 to 730 MPa and is controllable to adjusting the relative amount of npMA and EGDA.

Construction of air-gap structure using e-beam lithography

Scheme 2 illustrates the flowchart of fabrication of air-gap in the following sequence: (1) deposition of P(npMA-co-EGDA) on silicon wafer by iCVD, (2) application of PMMA e-beam resist by spincasting followed by pre-baking, (3) creation of desired pattern on PMMA layer by e-beam lithography, (4) exposing the desired pattern on PMMA layer by developing in mixture of isopropanol and methyl isobutyl ketone, rinsing in isopropanol and drying with nitrogen, (5) simultaneous stripping of PMMA resist and P(npMA-co-EGDA) sacrificial material by reactive ion etching to transfer the pattern to the latter, (6) deposition of silica overlay by PECVD, (7) thermal annealing to decompose polymer chains into small fragments so that they diffuse through the porous overlayer and leave the air-gap behind.



Scheme 2: Flowchart of construction of air-gap structure using e-beam lithography

Figure 36 shows the SEM photograph of the cross section of air-gap structure. The feature height and size are 100nm and. The surface of silica remained flat and was without crack, implying the

diffusion of small fragments, the product of thermal decomposition, was sufficiently rapid and no excessive pressure buildup occurred in the compartment that resulted in the catastrophic ruptures. The porosity of PECVD silica overlayer under the deposition conditions detailed in the section of experiment was determined to be 0.035 and 0.01 by BET absorption isotherm analysis and estimation based on the weight of the overlayer, respectively. The low porosity allows the fragments generated during the decomposition of sacrificial material to diffuse and the mechanical properties are expected not to compromise to any appreciable extent.

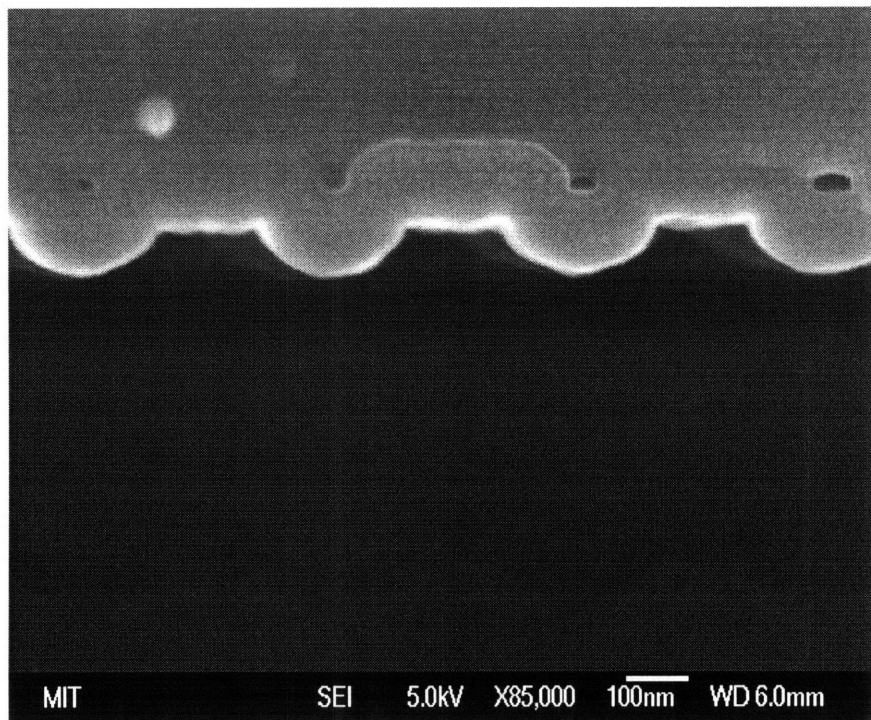


Figure 36: SEM image of air gap with feature size of 200nm and feature height of 100nm

The trapezoidal shape of the air-gap in fig. 36 was attributed to the rebound of the ions during RIE process. Although RIE process is highly anisotropic, ions with excessive kinetic energy are likely to sputter the materials on the sidewall, resulting in more isotropic trench and deformed feature. The circumstance is expected to be alleviated by tuning the power of radio frequency to reduce the energy of impinging ions and this is likely to be the key step of retaining the integrity of sacrificial materials of even smaller feature sizes.

Conclusion

A crosslinked copolymer, poly (neopentyl methacrylate-*co*-ethylene glycol diacrylate), abbreviated as P(npMA-*co*-EGDA), was developed and chosen as a potential candidate for air-gap sacrificial materials among a careful screening of over 20 types monomers and 4 types of crosslinkers and after detailed characterization of the thermal and mechanical properties. Initiated chemical vapor deposition made it possible to perform direct deposition of highly crosslinked copolymer onto the substrate with good uniformity and high deposition rate, as well as retain the chemical structure of resulting copolymer that is essentially the same as the polymer synthesized via conventional free-radical polymerization. By varying the composition of the copolymer, the removal percentage (93~98%), the onset temperature of decomposition (290~350 °C), Young's modulus (3.9~5.5 GPa) and hardness (0.38~0.75 GPa) of P(npMA-*co*-EGDA) can be adjusted. When the amount of monomers was increased, the mechanical properties and the onset temperature of decomposition gradually decreased while and removal percentage increased. The volatile product of thermal decomposition consisted of npMA monomer, homo- and hetero-dimer of npMA and EGDA and higher oligomers. The residue was composed of cyclic anhydride and aromatic moieties. The rate of decomposition was described well by logistic model and the activation energies of thermal decomposition of P(npMA-*co*-EGDA) was in the reasonable range of 162.7±8 kJ/mol and independent of copolymer composition. Fabrication of air-gap structure of feature size of 200 nm and feature height of 100 nm was achieved using PECVD-silica as overlayer; successful removal of P(npMA-*co*-EGDA) sacrificial material was achieved without damaging the integrity of the silica overlayer.

Reference

1. R. T. Conley, *Thermal stability of polymers*, vol. 1, Marcel Dekker, 1970, p.225.
2. S. L. Madorsky, *Thermal degradation of organic polymers*, Interscience publishers, 1964, chap. 7.
3. H. H. G. Jellinek, *Aspects of degradation and stabilization of polymers*, 1978, chap.6.
4. K. Pielichowski and B. Swierz-Motysia, *J. therm. anal. and calorimetry*, 83(1), pp.207~212, 2006.
5. G. Odian, *Principles of polymerization*, 3rd ed., John Wiley&Sons, 2001, pp252~253.
6. K. Chan and K. K. Gleason, *J. Electrochem. Soc.*, 153(4), C223~C228, 2006.
7. D. Bhusari, H. Reed, M. Wedlake, A. Padovani, S. A. Bidstrup Allen and P. A. Kohl, *J. microelectromechanical systems*, 10, 2001, pp. 400~409.
8. G. Moore, *Electronics Magazine*, 38(8), April 19, 1965.
9. C. C. Yang, P. T. Wu and W. C. Chen, *Polymer*, 45(16), 2004, pp. 5691~5702.
10. A. M. Padovani, L. Rhodes, L. Riester, G. Lohman, B. Tsuie, J. Conner, Allen SAB and P. A. Kohl, *Electrochem. Solid State Lett.*, 4(11), 2001, pp. F25~28.
11. G. S. Oehrlein, T. E. F. M. Standaert and P. J. Matsuo, *Solid State Technol.*, 43(5), 2000, p. 125.
12. L. Peters, *Editorial: Semiconductor International*, January 1, 2005.
13. J. Brinker and G. W. Scherer, *Sol-Gel Science*, Academic Press, London, 1990, chap. 3.
14. *Polym. degradation and Stab.*, 17(4), 1987, pp.327~339.
15. K. Demirelli, M. Coskun, E. Kaya, *J. Polym. Sci. Polym. Chem.*, 42(23), 2004, pp.5964~5973.
16. T. A. Sokolova and G. M. Chetyrkina, *Vysokomolekulyarnye Soedineniya*, , 3, 1961, pp.244~7.
17. P. S. Yu, V. N. Nikitin, M. V. Vol'kenshtein, *Zhurnal Strukturnoi Khimii*, 3(3), 1962, pp.287~91.
18. K. Yokota, J. Oda, *Kogyo Kagaku Zasshi*, 73(1), 1970, pp.224-8.
19. T. Otsu, M. Inoue, B. Yamada and T. Mori, *J. Polym. Sci. Polym. Lett. ed.*, 13(8), 1975, pp.505~10.
20. X. Xie and T. E Hogen-Esch, *Macromolecules*, 29, 1996, pp.1746~1752.

21. W. R. Marriot and E. Y. X. Chen, *Macromolecules*, 38(16), 2005, pp.6822~6832.
22. A. Matsumoto, S. Tanaka, T. Otsu, *Macromolecules*, 24(14), 1991, pp.4017-24.
23. N. Kato, Y. Kuroda, N. Tomino and K. Nakamura, *Netsu Kokasei Jushi*, 11(3), 1990, pp.131~143.
24. N. Kato and K. Nakamura, *Kobunshi Ronbunshu*, 46(5), 1989, pp.313~318.
25. K. Chan and K. K. Gleason, *Chemical Vapor Deposition*, 11(10), 2005, pp.437~443.
26. <http://mathworld.wolfram.com/LogisticEquation.html>
27. A. Asperger, W. Engewald and T. Wagner, *J. Anal. Appl. Pyrolysis*, 49, 1999, pp.155~164.
28. G. M. Pharr, W. C. Oliver and F. R. Brotzen, *J. Mater. Res.*, 7(3), 1992, pp.613~617.
29. B. Cruden, K. Chu, K. Gleason and H. Sawin, *J. Electrochem. Soc.*, 1999, p.4590.
30. <http://info.cas.org/SCIFINDER/scicover2.html>
31. M. Gupta and K. K. Gleason, *Langmuir*, 2006, pp.10047~10052.
32. T. P. Martin and K. K. Gleason, *Chemical Vapor Deposition*, 2006, 12, 11, pp. 685~691.
33. W. S. O'Shaughnessy, M. Gao and K. K. Gleason, *Langmuir*, 2006, pp.10047~10052.
34. K. Chan and K. K. Gleason, *Langmuir*, 2005, 21, p.8930.
35. Y. Mao and K. K. Gleason, *Langmuir*, 2004, 20, p.2484.
36. A. G. Emslie, F. T. Bonner and L. G. Peck, *J. Appl. Phys.*, 1958, 29, 5, pp. 858~862.
37. <http://www.cem.msu.edu/~cem924sg/XPSASFs.html>
38. J. F. Watts and J. Wolstenholme, *An introduction to surface analysis by XPS and AES*, Wiley, 2003, p. 13.
39. C. C. Chang and W. C. Chen, *Chem. Mater.*, 2002, 14, 10, pp. 4242~4248.
40. S. J. Kim, C. K. Lee and S. I. Kim, *High performance polymers*, 2002, 14, 4, pp. 351~362.
41. J. E. McGrath, L. Rasmussen, A. R. Shultz, H. K. Shobha, M. Sankarapandian, T. Glass, T. E. Long, A. J. Pasquale, *Polymer*, 2006, 47, 11, pp. 4042~4057.
42. S. Zulfiqar, N. Akhtar, M. Zulfiqar and I.C. McNeill, *Polymer degradation and stability*, 1989, 23, pp.299~308.

43. M. Principe, P. Ortiz and R. Martinez, *Polym International*, **1999**, 48, 8, pp. 637~641.
44. Q. T. Pham and R. Pétiand, *Proton and carbon NMR spectra of polymers*, 5th ed., **2003**, Wiley.
45. G. C. Lan, A. Maury and I. L. Yaacob, *Fracture and Strength of Solids VI, part 1 and 2, Key Eng. Mater.*, **2006**, 306-308, pp. 1061~1065.
46. D. P. Seraphim, R. Lasky and C. Y. Li, *Principles of Electronics Packaging*, **1989**, McGraw-Hill.
47. L. G. Gosset, A. Faarcy, J. de Pontcharra, Ph. Lyan, R. Daamen, G. J. A. M. Verheijden, V. Arnal, F. Gaillard, D. Bouche, P. H. L. Bancken, T. Vandeweyer, J. Michelon, V. Nguyen Hoang, R. J. O. M. Hoofman and J. Torres, *Microelectronic Engineering*, **2005**, 82, pp. 321~332.
48. R. Hoofman, R. Daamen, J. Michelon and V. Nguyenhoang, *Solid State Technology*, **2006**, 49, 8, pp. 35~38.
49. R. J. O. M. Hoofman, G. J. A. M. Verheijden, J. Michelon, F. Iacopi, Y. Travalay, M. R. Baklanov, Zs. Tőkei and G. P. Beyer, *Microelectronic Engineering*, **2005**, 80 pp. 337~344.